Part II
Specific Channel Types

2 Gramicidin Channels: Versatile Tools

Olaf S. Andersen, Roger E. Koeppe II, and Benoît Roux

2.1 Overview

Gramicidin channels are miniproteins in which two tryptophan-rich subunits associate by means of transbilayer dimerization to form the conducting channels. That is, in contrast to other ion channels, gramicidin channels do not open and close; they appear and disappear. Each subunit in the bilayer-spanning channel is tied to the bilayer/solution interface through hydrogen bonds that involve the indole NH groups as donors and water or the phospholipid backbone as acceptors. The channel's permeability characteristics are well-defined: gramicidin channels are selective for monovalent cations, with no measurable permeability to anions or polyvalent cations; ions and water move through a pore whose wall is formed by the peptide backbone; and the single-channel conductance and cation selectivity vary when the amino acid sequence is varied, even though the permeating ions make no contact with the amino acid side chains. Given the plethora of available experimental information—for not only the wild-type channels but also for channels formed by amino acid-substituted gramicidin analogues—gramicidin channels continue to provide important insights into the microphysics of ion permeation through bilayer-spanning channels. For similar reasons, gramicidin channels constitute a system of choice for evaluating computational strategies for obtaining mechanistic insights into ion permeation through the more complex channels formed by integral membrane proteins.

2.2 Introduction

Gramicidin channels are formed by the linear gramicidins, a family of peptide antibiotics produced by the soil bacillus *B. brevis* (Dubos, 1939; Hotchkiss, 1944), or by semisynthesis or total synthesis of gramicidin analogues (Bamberg et al., 1978; Morrow et al., 1979; Heitz et al., 1982; Greathouse et al., 1999). The linear gramicidins were the first antibiotics used in clinical practice (Herrell and Heilman, 1941). They exert their antibacterial activity by increasing the cation permeability of target bacterial plasma membranes (Harold and Baarda, 1967) through the formation of bilayer-spanning channels (Hladky and Haydon, 1970).

Compared to channels formed by many other antibiotics, the gramicidin channels are exceptionally well-behaved. Once formed, the bilayer-spanning channels have a single conducting state, which taken together with the channels' cation

selectivity (Myers and Haydon, 1972) and well-understood single-stranded (SS) $\beta^{6.3}$-helical structure (Urry, 1971, 1972; Arseniev et al., 1986; Ketchem et al., 1997; Townsley et al., 2001; Allen et al., 2003) make gramicidin channels important tools for understanding the physicochemical basis ion permeation through bilayer-spanning channels. Not surprisingly, the gramicidin channels have served as the prototypical channels in the development of many physical approaches toward understanding channel (or membrane protein) structure and function (Busath, 1993).

Gramicidin channels are arguably the best understood ion channels. Atomic (or near-atomic) resolution structures have been reported for an increasing number of complex ion channels formed by integral membrane proteins (Weiss et al., 1991; Cowan et al., 1992; Chang et al., 1998; Doyle et al., 1998; Bass et al., 2002; Jiang et al., 2002, 2003; Kuo et al., 2003; Long et al., 2005; Unwin, 2005). Yet the gramicidin channels embody a unique combination of features that sets them apart from other channels: first, the advantages construed by the wealth of information about the channel's ion permeability taken together with an atomic-resolution structure; second, the ion permeability can be modulated by defined chemical modifications whose influence on structure as well as function can be determined experimentally; finally, the wild-type and amino-substituted analogue channels are large enough to be nontrivial, yet small enough to be amenable to detailed computational studies.

In this chapter we first review the channel structure, dynamics, and function. We show that even though the linear gramicidins are conformationally polymorphic in organic solvents, they fold into one predominant conformer (the channel structure) in lipid bilayers and bilayer-like environments—yet the conformational preference may change in cases of extreme bilayer-channel hydrophobic mismatch. We then discuss the channels' permeability properties and show how it is possible to develop discrete-state models to describe the kinetics of ion movement through the channels. Finally, we briefly show how molecular dynamics (MD) simulations have advanced to the level of achieving semiquantitative agreement between observed and predicted ion permeabilities.

2.3 Structure

The linear gramicidins, exemplified by [Val^1]gramicidin A (gA), have an alternating (L-D)-amino acid sequence (Sarges and Witkop, 1965):

Formyl-L-Val^1-(D)-Gly-L-Ala^3-D-Leu-L-Ala^5-
-D-Val- L-Val^7-D-Val-L-Trp^9-D-Leu-L-Trp^{11}-
-D-Leu-L-Trp^{13}-L-Trp^{15}-ethanolamide.

(Only the L residues are numbered.) In *B. brevis*, the linear gramicidins are synthesized by nonribosomal peptide synthesis (Lipmann, 1980). The synthesis is catalyzed by a complex of four nonribosomal peptide synthases (Kessler et al., 2004), which

encompass a total of 16 modules that catalyze the successive activation and condensation (peptide bond formation) of amino acids to produce the specific sequence. The D-residues in the sequence are produced by epimerization of the corresponding L-residues. (For an overview of nonribosomal peptide synthesis, see Sieber and Marahiel, 2005.) The first module, which activates the amino-terminal L-Val, contains a putative formylation domain (Kessler et al., 2004). In the growing chain, the last amino acid is Gly; the peptide is released from the synthase template in a two-step NADH/NADPH-dependent reduction of this Gly to yield the carboxyterminal ethanolamide (Schracke et al., 2005). Due to relaxed substrate specificity in the first and eleventh modules, the naturally occurring gramicidin (gramicidin "D" after R. Dubos) is a mixture of [Val^1]- and [Ile^1]gramicidins A (with Trp^{11}), B (with Phe^{11}), and C (Tyr^{11}). [Val^1]gA constitutes about 70% of the natural mixture (as deduced from HPLC tracings in Koeppe et al., 1985).

For modern electrophysiological studies, the gramicidins are synthesized on peptide synthesizers using standard, solid-state peptide chemical methods (Killian et al., 1999). The synthesized products are purified, to a purity of better than 99%, using a two-stage reversed-phase HPLC procedure (Weiss and Koeppe, 1985). This is particularly important for single-channel experiments (Greathouse et al., 1999), which usually rely on the ability to identify the unique electrophysiological "fingerprints" of channels formed by different sequence-substituted gA analogues.

The alternating (L-D) gramicidin sequence allows the molecule to fold as a β-helix with the side chains projecting from the exterior surface of a cylindrical tube formed by the peptide backbone (Urry, 1971; Ramachandran and Chandrasekaran, 1972). Many such folding patterns are possible, and gA is conformationally polymorphic (Veatch et al., 1974). At least seven different helical conformers have been described in organic solvents (Veatch and Blout, 1974), where gA forms a variety of double-stranded (DS), intertwined dimers—the so-called ππ-helices (Bystrov and Arseniev, 1988; Langs, 1988; Abdul-Manan and Hinton, 1994; Burkhart et al., 1998).

In aqueous solutions, gA usually forms poorly defined aggregates (Kemp and Wenner, 1976). At very low aqueous concentrations, in the low picomolar range that is used in electrophysiological studies where the gramicidins usually are added to the aqueous solutions at the two sides of the bilayer, gA seems to fold into a stable monomer structure (Jagannadham and Nagaraj, 2005).

2.3.1 One Conducting Channel Conformation

In spite of the conformational polymorphism observed in organic solvents, gramicidin channels adopt a unique structure in lipid bilayer membranes or in bilayer-like environments (such as micelles, with a nonpolar/polar interface). The channel's electrophysiological "fingerprints" (single-channel current traces, Fig. 2.1; and current transition amplitude and lifetime distributions, Fig. 2.2) show that a single predominant conducting channel structure is formed by both the wild-type gA and the [D-Ala^2,Ser^3]gA analogue—and most other gA analogues.

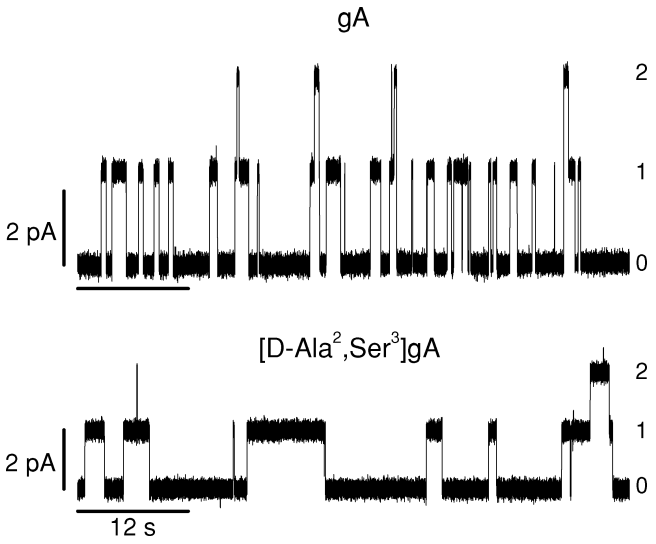

Fig. 2.1 Gramicidin single-channel current traces. Top: single-channel current trace obtained with gA. Bottom: single-channel current trace obtained with the gA analogue [D-Ala^2,Ser^3]gA. Both gA and [D-Ala^2,Ser^3]gA form one predominant type of ion-conducting channels, which are "visible" as discrete, well-defined transitions changes in the current through the membrane. The numbers to the right of the traces denote the number of conducting channels at the different current levels. The conducting states are "stable," meaning that the current noise of the conducting state is indistinguishable from that of the baseline. In the gA experiment, the root-mean-square (RMS) of the current in levels 0 through 2 varies between 0.148 and 0.150 pA; in the [D-Ala^2,Ser^3]gA experiment, the RMS of the current in levels 0 through 2 varies between 0.133 and 0.136 pA. The experimental methods were done as described in Greathouse et al. (1999). Experimental conditions: diphytanoylphosphatidylcholine/*n*-decane bilayers; electrolyte solution, 1.0 M NaCl, pH 7; applied potential 200 mV; current signal filtered at 500 Hz.

Both the single-channel current transition amplitudes and channel lifetimes vary when the amino acid sequence is varied; different gA analogues usually form channels with distinct electrophysiological characteristics—even though the amino acid side chains do not come in direct contact with the permeating ions. For example, the Gly$^2 \rightarrow$ D-Ala^2 substitution by itself causes a 10–15% increase in the single-channel current transition amplitude and a fourfold increase in the average channel lifetime (τ) (Mattice et al., 1995). The Ala$^3 \rightarrow$ Ser^3 substitution behaves similarly to other polar amino acid substitutions in the formyl-NH-terminal half of the sequence (Morrow et al., 1979; Russell et al., 1986; Durkin et al., 1990; Koeppe et al., 1990), to cause reductions in both the current transition amplitude and lifetime.

On occasion, one may observe transitions between two different current levels in a "stable" bilayer-spanning gA channel (Busath and Szabo, 1981). Some reports also have suggested that up to 25–50% of channels formed by purified gA may be variants (affectionately called "minis") whose current transition amplitudes fall above or (usually) below the main peak (Hladky and Haydon, 1972; Busath and Szabo, 1981;

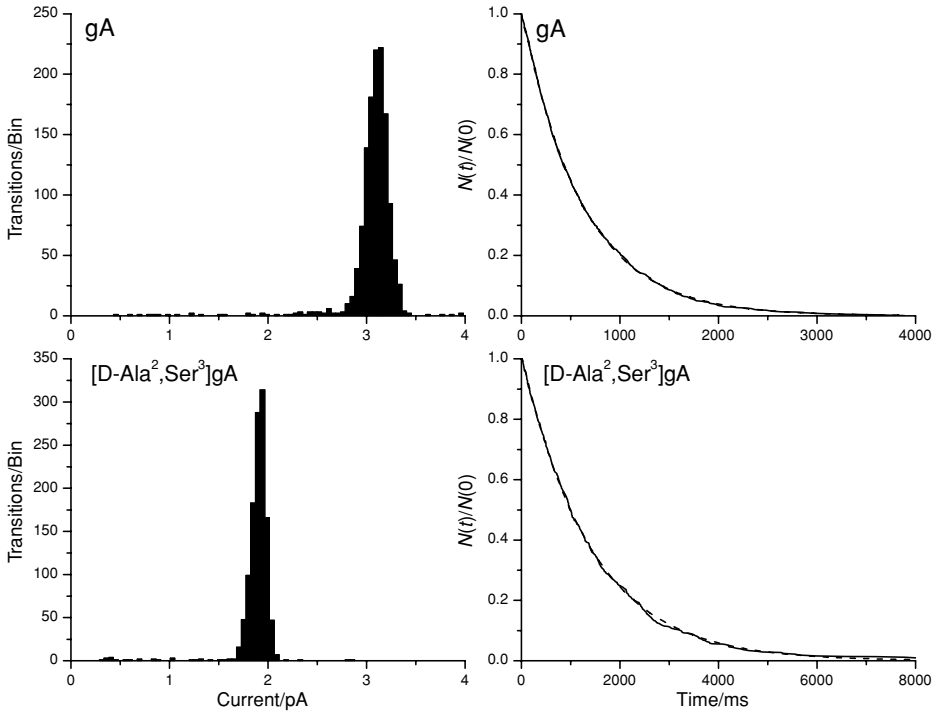

Fig. 2.2 Characterization of gramicidin channel function. Top: results for gA channels. Bottom: results for [D-Ala^2,Ser^3]gA channels. Left: current transition amplitude histograms. The single predominant peaks around 3.1 pA (for gA channels) and 1.9 pA (for [D-Ala^2,Ser^3]gA channels) comprise 1246 out of 1294 transitions (for gA) and 1175 out of 1202 transitions (for [D-Ala^2,Ser^3]gA), meaning that we can account for 96–97% of the observed current transitions. Right: lifetime distributions as normalized survivor plots; note the twofold difference in the scale in the abscissa. The interrupted curves are fits of $N(t)/N(0) = \exp\{-t/\tau\}$ to the results, where $N(t)$ is the number of channels with lifetime longer than time t, and τ is the average lifetime (610 ms for gA channels and 1410 ms for [D-Ala^2,Ser^3]gA channels). Experimental conditions as in Fig. 2.1.

Urry et al., 1984). Though the structural basis for these conductance variants remains enigmatic, they somehow result from subtle experimental "artifacts" (Busath et al., 1987). They will not be considered further here.

In addition to establishing that there is a single predominant channel conformation, electrophysiological and other functional studies provided important structural constraints that were instrumental in establishing the subunit fold. Based upon the channel's permeability to alkali metal cations, H^+ and water, and its impermeability to urea (Hladky and Haydon, 1972; Myers and Haydon, 1972; Finkelstein, 1974), it was concluded that the peptide backbone surrounds an aqueous pore with luminal diameter ~4 Å. Even among the β-helices, different folding patterns with ~4.4 and ~6.3 residues per turn are possible. The functional results allowed for refinement of the originally proposed β-helical structure (Urry, 1971), eventually leading to a

$\beta^{6.3}$-helical structure with ∼6.3 residues per helical turn (Urry, 1972). Together with results from gA-dependent conductance relaxations (Bamberg and Läuger, 1973), single-channel experiments on modified gramicidins (Bamberg et al., 1977; Veatch and Stryer, 1977; Cifu et al., 1992) and nuclear magnetic resonance (NMR) spectroscopy on labeled gramicidins (Weinstein et al., 1979, 1980), the constraints imposed by the physiological results established gA channels to be antiparallel SS $\beta^{6.3}$-helical dimers. More details concerning the early structural and functional evidence for this structure are summarized in Andersen and Koeppe (1992) and Andersen et al. (1999).

The SS $\beta^{6.3}$-helical channel structure is remarkably resilient to a large variety of single amino acid substitutions in the gA sequence (Mazet et al., 1984; Russell et al., 1986; Durkin et al., 1990; Becker et al., 1991; Fonseca et al., 1992; Koeppe et al., 1994a; Mattice et al., 1995; Koeppe and Andersen, 1996; Killian et al., 1999), but see also Durkin et al. (1992) and Andersen et al. (1996). This structural resilience makes gA channels valuable as prototypical channels.

2.3.2 Atomic Resolution Structure

The atomic resolution structure was determined by independent solution and solid-state NMR experiments (Arseniev et al., 1986; Ketchem et al., 1997; Townsley et al., 2001). Though the solution NMR studies were done on gA incorporated into sodium dodecylsulfate micelles (SDS) and the solid-state NMR experiments were done on gA incorporated into oriented dimyristoylphosphatidylcholine (DMPC) bilayers, the results have converged to agreement upon one channel structure (Fig. 2.3). The channel is an antiparallel formyl-NH-terminal-to-formyl-NH-terminal dimer (Cross et al., 1999) formed by right-handed (RH), SS $\beta^{6.3}$-helical subunits, which are joined by six intermolecular hydrogen bonds (Fig. 2.4). Minor differences between the reported Protein Data Bank (PDB) structures, based on solid-state and solution NMR (PDB:1MAG and PDB:1JNO, respectively), can be reconciled through molecular dynamics analysis of the structures (Allen et al., 2003) and by considerations of degenerate Trp side-chain conformations that satisfy the solid-state NMR data (Koeppe et al., 1994b; Hu and Cross, 1995).

The intermolecular hydrogen bonds at the subunit interface that stabilize the bilayer-spanning dimer in RH $\beta^{6.3}$-helices are formed between the L-residues in the two subunits (Fig. 2.4); they are topologically equivalent to those of antiparallel β-sheets. By contrast, the intramolecular hydrogen bonds that define the subunit fold are topologically equivalent to those of parallel β-sheets (Urry, 1971). Apart from the helix being right-handed, rather than left-handed, the structure is remarkably similar to the one proposed by D.W. Urry more than 30 years ago (Urry, 1971, 1972).

An atomic resolution structure is available only for the gA dimer, not for the nonconducting monomer. Small-angle x-ray scattering experiments on *t*-BOC-gA (He et al., 1994), with the formyl group replaced by a *tert*-butyloxycarbonyl moiety, which destabilizes the ion-conducting dimer by some five orders of magnitude

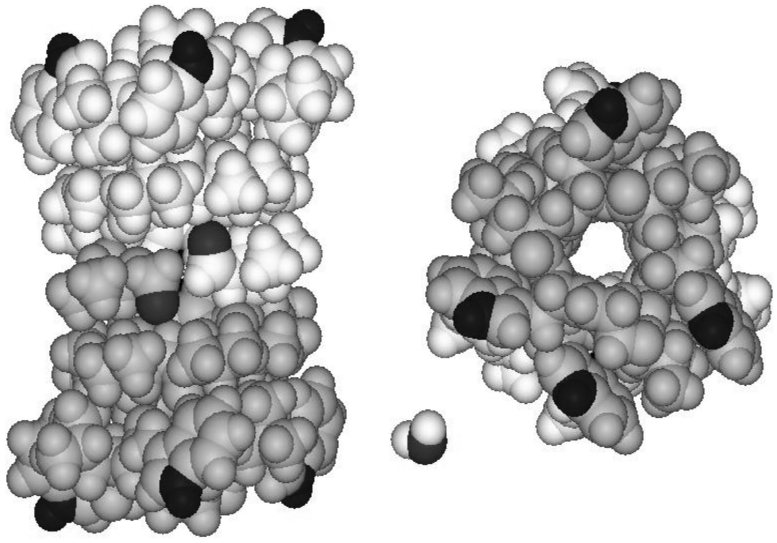

Fig. 2.3 Side and end views of the bilayer-spanning gramicidin A channel. The energy-minimized structure represents a composite that is consistent with the several NMR-determined structures (Arseniev et al., 1986; Ketchem et al., 1997; Townsley et al., 2001). The two subunits are shaded differently. The formyl oxygens and indole NH's are black. The four Trp indole rings cluster near each membrane/solution interface. (A water molecule is shown for comparison.)

relative to gA, show that bilayer-incorporated monomers also fold into $\beta^{6.3}$-helices. These monomers are imbedded in the bilayer with their (average) axis orientation parallel to the bilayer normal.

Even though the gA channel weighs in at only ∼4 kDa, the results in Figs. 2.1–2.3 show that gA channels have the structural and functional definitions expected for more complex membrane proteins. These combined features continue to put gA channels in a class of their own. In fact, the current transitions in Fig. 2.1 show less "excess noise" than the current transitions observed in channels formed by integral membrane proteins, e.g., KcsA channels (Nimigean and Miller, 2002) or Ca^{2+}-activated potassium channels (Park et al., 2003). With gramicidin channels, one therefore can with some certainty relate the measured function to a specific, albeit dynamic (Allen et al., 2003), structure. Gramicidin channels should be considered to be miniproteins!

2.3.3 Importance of the Tryptophans for Channel Structure

The four Trp residues in each subunit are important determinants of the channel fold because the indole NH groups seek to form hydrogen bonds to polar residues at the bilayer/solution interface (O'Connell et al., 1990), which would favor SS over DS conformers (Durkin et al., 1992). The propensity for Trp to avoid the bilayer center is further highlighted by the very short lifetimes of channels formed by gramicidins

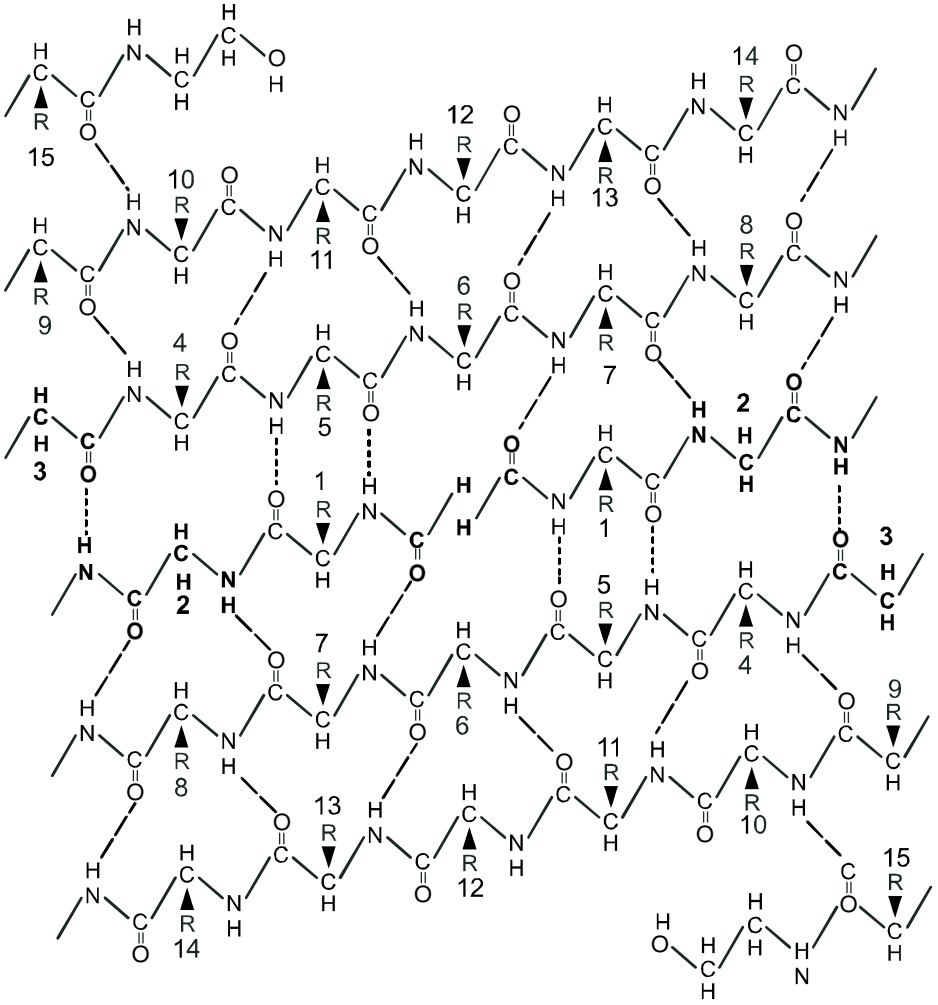

Fig. 2.4 Hydrogen bond organization in the membrane-spanning, right-handed $\beta^{6.3}$-helical dimer. The intramolecular hydrogen bonds that stabilize each $\beta^{6.3}$-helical subunit are denoted by – –. The six intermolecular hydrogen bonds that stabilize the subunit interface are denoted by - - -. The residues in each subunit are numbered; residues 2 and 3, which were modified in [D-Ala^2,Ser^3]gA are in **bold**.

that have N-formyl-Trp^1 instead of N-formyl-Val^1 (Mazet et al., 1984). Indeed, the conformational plethora observed in organic solutes shows that the intrinsic gA folding preference is to form intertwined DS structures in which the Trp residues are distributed along the dimer surface (Fig. 2.5).

In a lipid bilayer or bilayer-like environment, nevertheless, the folding preference becomes dramatically altered, driven by the energetic necessity to rearrange the Trp indole rings (cf. Figs. 2.3 and 2.5). When the DS conformers encounter lipid

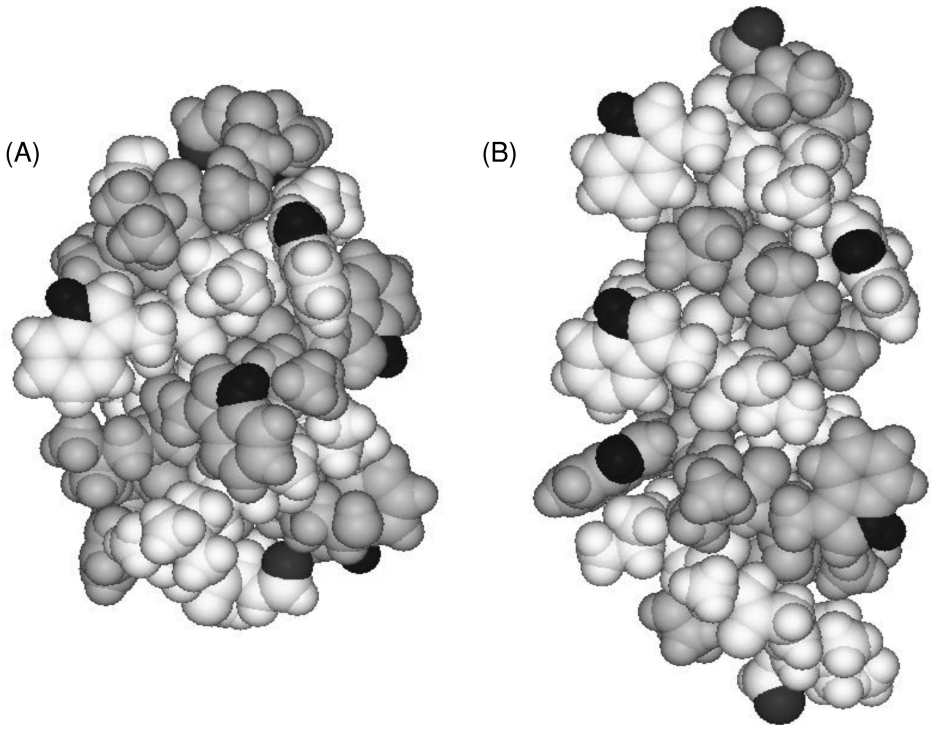

Fig. 2.5 Side views of two antiparallel DS gA conformers crystallized from organic solvents. (A) The $\vec{\pi}\overleftarrow{\pi}^{7.2}$ structure, with 7.2 residues per helical turn, crystallized from CsCl/methanol or from acetic acid, PDB:1AV2 (Burkhart et al., 1998). (B) The $\vec{\pi}\overleftarrow{\pi}^{5.6}$ structure, with 5.6 residues per helical turn, crystallized from ethanol, PDB:1ALZ (Langs, 1988). As in the $\beta^{6.3}$-helical structure in Fig. 2.3, the two subunits are shaded differently, and the formyl oxygens and indole NH's are black. In contrast to Fig. 2.3, the Trp indole rings in the DS structures do *not* cluster near the ends (the membrane/solution interfaces), but are distributed quite evenly along the dimer.

bilayer membranes, they unfold/refold into the Trp-anchored SS structure in Fig. 2.3 (Andersen et al., 1999). In electrophysiological single-channel experiments, the conducting channels form by the transbilayer dimerization of two nonconducting ($\beta^{6.3}$-helical) subunits (O'Connell et al., 1990)—as opposed to a direct interconversion of nonconducting DS dimers to conducting SS dimers. In this $\beta^{6.3}$-helical conformation, the seemingly very hydrophobic (Segrest and Feldmann, 1974) gA molecules cross lipid bilayers poorly (O'Connell et al., 1990)—providing further evidence for the importance of the hydrogen bond-stabilized anchoring to the bilayer/solution interface.

The preference to fold into SS channels in lipid bilayers, and in bilayer-like environments, arises from the energetic penalty associated with burying the Trp indole rings in the bilayer hydrophobic core, as observed initially with [Trp^1]gA (Mazet et al., 1984). Furthermore, gA analogues with multiple Trp→Phe substitutions form a variety of DS structures in lipid bilayers (Salom et al., 1995, 1998; Rawat et al.,

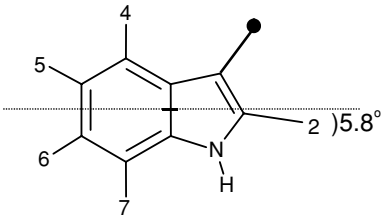

Fig. 2.6 Trp indole ring geometry with the positions of deuteration numbered; after Pulay et al. (2005). The indole ring geometry was determined from ab initio calculations and experimental ^{2}H-NMR spectra (Koeppe et al., 2003). A critical geometric feature is the 5.8° angle of the C2–^{2}H bond with respect to the normal to the ring bridge.

2004). These DS conformers generally are nonconducting, although some specialized combinations of Trp→Phe substitutions together with changes in backbone length and side-chain stereochemistry can lead to the formation of DS conducting channels (Durkin et al., 1992).

The interfacial localization of Trp, and Tyr, in gA channels seems to be a general characteristic of membrane proteins (Schiffer et al., 1992; Cowan and Rosenbusch, 1994; Killian and von Heijne, 2000). The organization of Trp and Tyr residues in integral membrane proteins presumably is due to the same energetic principles that have been deduced from the detailed analysis of gA channels.

The characterization of the orientations and dynamics of the Trp indole rings has been facilitated by solid-state ^{2}H-NMR spectra from gramicidins with labeled tryptophans, which have been incorporated into oriented multilayers (Cross, 1994; Davis and Auger, 1999). In addition to providing information about the dynamics of the gramicidin channels, these studies also have led to an improved understanding of the indole ring geometry—specifically the C2–H bond angle (Koeppe et al., 2003). Ab initio calculations, together with analysis of experimentally observed quadrupolar splittings from ^{2}H-NMR spectra, have converged to reveal that the indole C2–H bond makes an angle of 5.8° with respect to the normal to the bridge between the 5- and 6-membered rings (Fig. 2.6) (Koeppe et al., 2003).

Further calculations have established all of the tensor elements of the electric field gradient for each carbon–deuterium bond in the ring of deuterated 3-methylindole (Pulay et al., 2005). The off-bond tensor elements permit one to calculate an asymmetry parameter $\eta = (|V_{yy}| - |V_{xx}|)/|V_{zz}|$ for each position on the indole ring. These asymmetry parameters in turn allow for improved descriptions of the average orientation and dynamics of each of the four Trp indole rings that anchor gA channels in their transmembrane orientation (Fig. 2.3), which in turn allows for detailed descriptions of not only the average orientations but also the dynamics of backbone and side chains (Pulay et al., 2005). These developments could be implemented because of the unique advantages conferred by gA, and they have implications for understanding the average orientation, dynamics, and functional role(s) of Trp residues in integral membrane proteins.

At the NMR time scale, the bilayer-spanning gramicidin channels have their pore axes remarkably parallel to the bilayer normal (Nicholson et al., 1987; Cornell et al., 1988; Killian et al., 1992). From solid-state NMR spectra, the average wobble is zero and the principal order parameter is 0.93 (Separovic et al., 1993). The outer pair of Trp residues (#13 and #15) have principal order parameters identical to the backbone order parameter (Pulay et al., 2005). The inner pair of Trp residues (#9 and #11) wobble only slightly more than the backbone (Pulay et al., 2005). Additionally, there may be rapid transitions of Trp^9 between different "conventional" rotamer positions (Allen et al., 2003). The four Val side chains likewise occupy canonical rotamer positions, with two rigid and two hopping (Lee et al., 1995). Two rotamers have been modeled for Trp^9 in lipid bilayers (Koeppe et al., 1994b; Ketchem et al., 1997), one of which is similar to the dominant rotamer in SDS micelles (Arseniev et al., 1986; Townsley et al., 2001). As shown by MD analysis of the Ketchem et al. and the Townsley et al. structures (Allen et al., 2003), both Trp^9 rotamers are compatible with a variety of solid-state NMR measurements. A weighted average, with rapid interconversion between the rotamers, is compatible with not only MD simulations but with fluorescence results that suggest that two of the Trps quench each other (Scarlata, 1988; Mukherjee and Chattopadhyay, 1994).

2.3.4 Importance of the Bilayer-Channel Hydrophobic Match

The shift in conformational preference between the polymorphic behavior in organic solvents and the unique structure in lipid bilayers is but one example of environment-dependent folding. Because the conducting channels form by the transbilayer dimerization of two nonconducting subunits (Fig. 2.7), the preference to fold into SS $\beta^{6.3}$-helical dimers, for example, depends on the hydrophobic "match" between bilayer thickness and channel length (Greathouse et al., 1994; Mobashery et al., 1997; Galbraith and Wallace, 1998).

Specifically, if the length of the channel's hydrophobic exterior (l) is much greater (Greathouse et al., 1994) or much less (Mobashery et al., 1997; Galbraith and Wallace, 1998) than the average hydrophobic thickness of the unperturbed host bilayer (d_0), then gA may fold into structures other than the standard SS $\beta^{6.3}$-helical dimers.

This bilayer thickness-dependent folding preference arises because: first, the energetic cost associated with exposing hydrophobic residues to water (Kauzmann, 1957; Tanford, 1980; Engelman et al., 1986; Dill, 1990; Sharp et al., 1991; White and Wimley, 1999) is substantial, varying between 2.5 and 7.5 kcal mol^{-1} nm^{-2}) (Dill et al., 2005); and second, lipid bilayers are not just thin sheets of liquid hydrocarbon, stabilized by the polar head groups, but liquid crystals with well-defined material properties. Fully hydrated, liquid-crystalline phospholipid bilayers are elastic bodies with volumetric compressibility moduli that are of the order of $\sim 10^9$ N m^{-2} (Liu and Kay, 1977; Tosh and Collings, 1986)—one to two orders of magnitude less than the moduli for globular proteins in water (Gekko and Noguchi, 1979). Because lipid

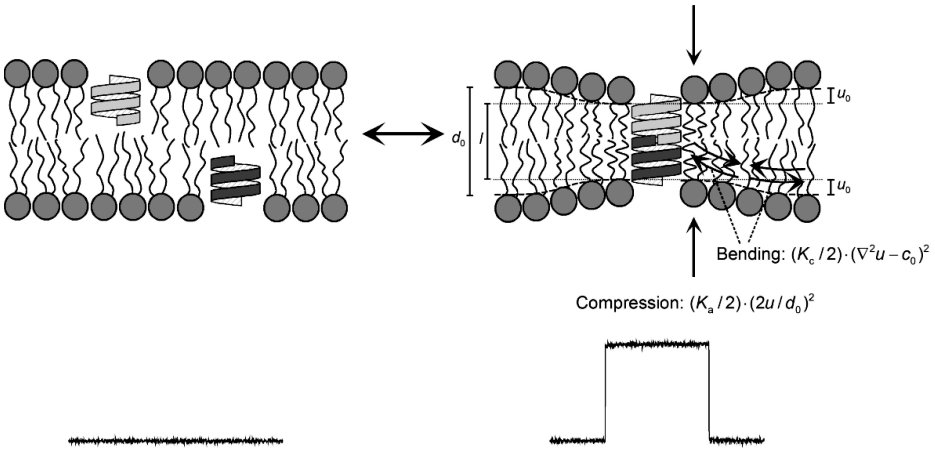

Fig. 2.7 gA channels form by the transbilayer dimerization of two RH, SS $\beta^{6,3}$-helical subunits. Top: schematic representation of the kinetics of channel appearance/disappearance (association/dissociation). Bottom: the associated current signals. When the channel's hydrophobic length (l) differs from the average thickness of the unperturbed bilayer hydrophobic core (d_0), channel formation will be associated with a bilayer deformation, which can be decomposed into the compression (with energy density $(K_a/2)\cdot(2u/d_0)^2$) and bending (with energy density $(K_c/2)\cdot(\nabla^2 u - c_0)^2$) of the two bilayer leaflets (Huang, 1986), where K_a and K_c denote the bilayer compression and bending moduli and $2u$ the local bilayer deformation.

bilayers are more flexible than the imbedded proteins (see below), the host lipid bilayer will deform whenever the hydrophobic length of a bilayer-spanning protein differs from the average thickness of the unperturbed bilayer (Owicki et al., 1978; Mouritsen and Bloom, 1984), cf. Fig. 2.7.

In principle, both the bilayer and the protein will deform in response to a hydrophobic mismatch, $d_0 \neq l$. In practice, the proteins can be approximated as being rigid bodies because lipid bilayers are very soft materials. The area expansion moduli (K_a) for liquid-crystalline phospholipid bilayers are $\sim$250 mN m^{-1} (Rawicz et al., 2000), and the bilayer hydrophobic thickness is $\sim$3 nm (Lewis and Engelman, 1983; Simon and McIntosh, 1986; Rawicz et al., 2000) meaning that the moduli for bilayer thickness compressibility, which is given by K_a/d_0 is $\sim 10^{-8}$ N m^{-2}, cf. Evans and Hochmuth (1978). That is, lipid bilayers are 100- to 1000-fold softer than the imbedded proteins. Because lipid bilayers are so soft, the bilayer/solution interface undergoes substantial thermal fluctuations (Wiener and White, 1992), which involve the local movement of individual phospholipid molecules, as well as more global bilayer undulations and peristaltic motions (Wiener and White, 1992; Lindahl and Edholm, 2000). The bilayer/solution interface thus is "fuzzy"; but the *average* bilayer thickness, which is relevant here, is a well-defined parameter.

The bilayer thickness-dependent folding arises because a bilayer deformation has an associated energetic cost, the bilayer deformation energy (ΔG^0_{def}) (Huang,

1986), which contributes to the overall free energy change (ΔG^0_{tot}) associated with the gA monomer↔dimer equilibrium (Fig. 2.7):

$$\mathsf{M} + \mathsf{M} \underset{k_{-1}}{\overset{k_1}{\rightleftharpoons}} \mathsf{D}$$

Scheme I

where M and D denote the nonconducting monomers (one in each bilayer leaflet) and conducting dimers, respectively. The dimerization constant (K_D) is given by

$$K_{\text{D}} = \frac{k_1}{k_{-1}} = \frac{[\mathsf{D}]}{[\mathsf{M}]^2} = \exp\left\{\frac{-\Delta G^0_{\text{tot}}}{k_{\text{B}}T}\right\} = \exp\left\{\frac{-\left(\Delta G^0_{\text{prot}} + \Delta G^0_{\text{def}}\right)}{k_{\text{B}}T}\right\}, \qquad (2.1)$$

where ΔG^0_{prot} denotes the free energy contributions that arise from the channel (protein) per se, k_{B} Boltzmann's constant, T the temperature in Kelvin, and [M] and [D] the mole-fractions of gA monomers and dimers in the bilayer. The ΔG^0_{def} contribution to ΔG^0_{tot} arises from the cost of the bilayer compression and monolayer bending that occur when the bilayer-spanning dimer forms (Huang, 1986; Nielsen and Andersen, 2000), cf. Fig. 2.7:

$$\begin{aligned}\Delta G^0_{\text{def}} = &\int_{r_0}^{\infty} \left\{K_{\text{a}} \cdot (2u/d_0)^2 + K_{\text{c}} \cdot (\nabla^2 u - c_0)^2\right\} \cdot \pi \cdot dr \\ &- \int_{r_0}^{\infty} K_{\text{c}} \cdot (\nabla^2 u - c_0)^2 \cdot \pi \cdot dr, \end{aligned} \qquad (2.2)$$

where r_0 is the channel radius, K_{a} and K_{c} the bilayer compression and bending moduli, $2u$ the local channel-bilayer mismatch ($u = (d - l)/2$, where d is the local bilayer thickness, is the local monolayer deformation) and c_0 the intrinsic (or spontaneous) monolayer curvature (Gruner, 1985). Eq. 2.2 can be expressed as (Nielsen et al., 1998; Nielsen and Andersen, 2000; Lundbæk et al., 2004):

$$\Delta G_{\text{def}} = H_{\text{B}} \cdot (d_0 - l)^2 + H_{\text{X}} \cdot (d_0 - l) \cdot c_0 + H_{\text{C}} \cdot c_0^2, \qquad (2.3)$$

where the coefficients H_{B}, H_{X}, and H_{C} are functions of K_{a}, K_{c}, d_0 and r_0 (Nielsen et al., 1998). The thickness-dependent conformational preference thus arises because ΔG^0_{def} varies as a function of $(d_0 - l)^2$. As $|d_0 - l|$ increases, the energetic penalty for inserting a bilayer-spanning SS dimer increases, eventually becoming so large that other conformers, including various DS structures, become favored (Greathouse et al., 1994; Mobashery et al., 1997; Galbraith and Wallace, 1998).

Given this context, the RH, SS $\beta^{6.3}$-helical (dimer) conformation is remarkably robust: it is preserved in bilayers with acyl chain lengths varying between C_{10}

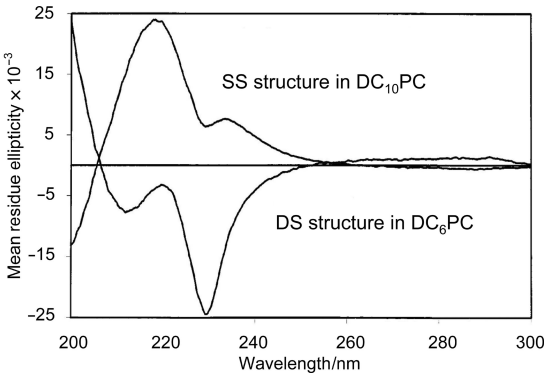

Fig. 2.8 CD spectroscopic "signatures" for the channel conformation of gA in Di-C_{10}-PC bilayers, and for the nonchannel (intertwined, DS) conformation in Di-C_6-PC micelles. Adapted from Greathouse et al. (1994).

and $C_{20:1}$ (Cornell et al., 1989; Greathouse et al., 1994; Mobashery et al., 1997; Galbraith and Wallace, 1998), and even in sodium dodecyl sulfate (SDS) micelles (Arseniev et al., 1986; Townsley et al., 2001; Allen et al., 2003). Fig. 2.8 shows the characteristic circular dichroism (CD) signatures for gA incorporated into di-C_{10}-phosphatidylcholine ($DC_{10}PC$), where it is in the RH, SS $\beta^{6.3}$-helical channel conformation, and into DC_6PC, where it is in a DS conformation.

2.3.5 Structural Equivalence of gA Mutants

Not only is the channel structure remarkably stable and well-defined, but the basic fold and peptide backbone organization also do not vary when the amino acid sequence is varied (as long as the alternating L-D-sequence, and the aromatic–aliphatic organization in the carboxy-ethanolamide half of the sequence, are maintained).

To test whether a mutant gramicidin, e.g. [D-Ala^2,Ser^3]gA, forms channels that are structurally equivalent to the native gA channels, one can exploit the following features (Durkin et al., 1990): first, gA channels are symmetric, antiparallel dimers formed by the transmembrane association of nonconducting, $\beta^{6.3}$-helical subunits residing in each leaflet of the bilayer (Fig. 2.7); and second, gA analogues usually form only a single channel type. Then, if two different gA analogues (A and B) form symmetric, homodimeric (AA and BB) channels that have the same structure, meaning the same peptide backbone fold, one should be able to observe the formation of asymmetric, heterodimeric (AB and BA) channels (Veatch and Stryer, 1977; Durkin et al., 1990, 1993). If the AA and BB channels differ in their current transition amplitudes, the heterodimeric (AB or BA) channels would be expected to have current transition amplitudes in between those of the homodimeric AA and BB channels. In general, if the potential of mean force for ion movement through the heterodimeric channels is asymmetric, which almost invariably is the case, the current in the A→B direction will differ from the current in the B→A direction. (In the limit where the

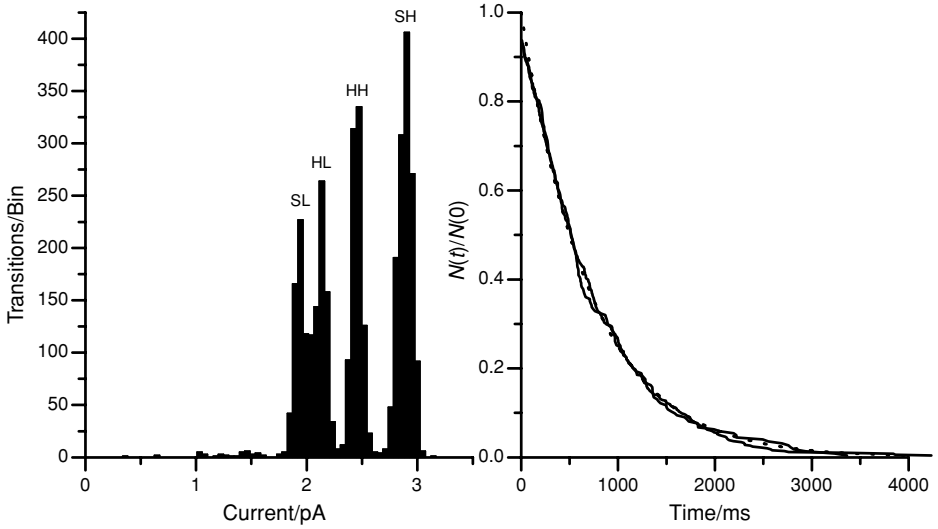

Fig. 2.9 Structural equivalence of gA and [D-Ala^2,Ser^3]gA channels. Left: current transition amplitude histogram obtained when [D-Ala^2,Ser^3]gA and gA both were added to both sides of a lipid bilayer. The four peaks represent (labeled from left to right): SL (symmetric low conductance) denotes [D-Ala^2,Ser^3]gA homodimers (at ∼1.9 pA); HL (hybrid low conductance) denotes [D-Ala^2,Ser^3]gA/gA heterodimers (at ∼2.2 pA); HH (hybrid high conductance) denotes gA/[D-Ala^2,Ser^3]gA heterodimers (at ∼2.5 pA); and SH (symmetric high conductance) denotes gA homodimers (at ∼2.9 pA). Right: lifetime distributions for the heterodimeric [D-Ala^2,Ser^3]gA/gA and gA/[D-Ala^2,Ser^3]gA channels. The interrupted curves are fits of $N(t)/N(0) = \exp\{-t/\tau\}$ to the results, where $N(t)$ is the number of channels with lifetime longer than time t, and τ is the average lifetime (770 ms for [D-Ala^2,Ser^3]gA/gA channels and 750 ms for gA/[D-Ala^2,Ser^3]gA channels). Experimental conditions as in Fig. 2.1.

applied voltage (V) $\rightarrow$0, the current, or more precisely the conductance, will be the same in the two directions.)

Figure 2.9 shows results from an experiment with the wild-type gA and the [D-Ala^2,Ser^3]gA analogue.

In the current transition amplitude histogram (Fig. 2.9A), there are four peaks. In addition to the symmetric gA/gA and [D-Ala^2,Ser^3]gA/[D-Ala^2,Ser^3]gA peaks (at ∼2.9 and ∼1.9 pA, respectively), which can be identified by comparison to the results with just a single gramicidin (Figs. 2.1 and 2.2), there are two new peaks (at ∼2.2 and ∼2.5 pA, respectively). These new peaks represent the [D-Ala^2,Ser^3]gA/gA and gA/[D-Ala^2,Ser^3]gA heterodimeric channels, respectively. The identities of the heterodimers were determined by adding [D-Ala^2,Ser^3]gA to only side of a bilayer and gA to only the other side, which defines the orientation of the heterodimeric channels because the gA and gA analogues cross lipid bilayers very poorly (O'Connell et al., 1990; Fonseca et al., 1992).

Formally, heterodimer (hybrid channel) formation can be described as the interconversion between two symmetric homodimeric channel types (AA and BB) and

the corresponding asymmetric heterodimeric channel types (AB and BA), cf. Durkin et al. (1990):

$$\mathrm{AA} + \mathrm{BB} \rightleftarrows \mathrm{AB} + \mathrm{BA}.$$

Scheme II

The equilibrium constant (K) for heterodimer formation is given by (Durkin et al., 1993)

$$K = \frac{[\mathsf{AB}] \cdot [\mathsf{BA}]}{[\mathsf{AA}] \cdot [\mathsf{BB}]}, \tag{2.4}$$

and the standard free energy for heterodimer formation ($\Delta\Delta G^0$) is defined as

$$\begin{aligned}\Delta\Delta G^0 &= -k_\mathrm{B}T \cdot \ln\{K\} = -\frac{k_\mathrm{B}T}{2} \cdot \ln\left\{\frac{K_\mathrm{AB} \cdot K_\mathrm{BA}}{K_\mathrm{AA} \cdot K_\mathrm{BB}}\right\} \\ &= \frac{(\Delta G^0_\mathrm{AB} + \Delta G^0_\mathrm{BA}) - (\Delta G^0_\mathrm{AA} + \Delta G^0_\mathrm{BB})}{2},\end{aligned} \tag{2.5}$$

where K_AB and ΔG^0_AB denote the association constant and standard free energy of formation for AB (the reaction $\mathsf{A} + \mathsf{B} \rightleftarrows \mathsf{AB}$), and so on. (The factor 1/2 arises because we wish to measure $\Delta\Delta G^0$ per mole of heterodimer, or subunit interface, cf. Durkin et al., 1990, 1993.)

The time-averaged "concentration" (channels/bilayer area) of AB is given by:

$$[\mathsf{AB}] = f_\mathsf{AB} \cdot \tau_\mathsf{AB}, \tag{2.6}$$

where $f_\mathsf{AB}(= k_\mathsf{AB} \cdot [\mathsf{A}] \cdot [\mathsf{B}])$ and $\tau_\mathsf{AB}(= 1/k_{-\mathsf{AB}})$ denote the channel appearance rate and lifetime, and k_AB and $k_{-\mathsf{AB}}$ are the association and dissociation rate constants. $\Delta\Delta G^0$ thus can be expressed in terms of experimental observables as

$$\Delta\Delta G^0 = -\frac{k_\mathrm{B}T}{2} \cdot \ln\left\{\frac{(f_\mathsf{AB} \cdot \tau_\mathsf{AB}) \cdot (f_\mathsf{BA} \cdot \tau_\mathsf{BA})}{(f_\mathsf{AA} \cdot \tau_\mathsf{AA}) \cdot (f_\mathsf{BB} \cdot \tau_\mathsf{BB})}\right\}. \tag{2.7}$$

The activation energy for heterodimer formation relative to the symmetric channels ($\Delta\Delta G^\ddagger_\mathrm{f}$) can be defined (and determined) by a reasoning that parallels the above:

$$\Delta\Delta G^\ddagger_\mathrm{f} = -\frac{k_\mathrm{B}T}{2} \cdot \ln\left\{\frac{f_\mathsf{AB} \cdot f_\mathsf{BA}}{f_\mathsf{AA} \cdot f_\mathsf{BB}}\right\}. \tag{2.8}$$

If $\Delta\Delta G^\ddagger_\mathrm{f} = 0$, there are no subunit-specific barriers to the formation of heterodimers, as compared to homodimers (Durkin et al., 1990, 1993), meaning that the different

subunits have the same fold. In this case, the distribution between the AA, BB, AB, and BA channels will be given by (Durkin et al., 1993):

$$f_{AB} \cdot f_{BA} = f_{AA} \cdot f_{BB}. \tag{2.9}$$

If also $\Delta\Delta G^0 = 0$, there are no subunit-specific interactions between the different subunits in the bilayer-spanning dimers, meaning that AA and BB are structurally equivalent (Durkin et al., 1990, 1993).

The relative heterodimer appearance rates in Fig. 2.9 conform to the predictions of Eq. 2.9, as $f_{AB} \cdot f_{BA}/(f_{AA} \cdot f_{BB}) = 0.96$ (or $\Delta\Delta G_f^{\ddagger} \approx 0$ kcal mol^{-1}). We therefore conclude that the Ala→Ser (and Gly→D-Ala) substitutions are well tolerated within the $\beta^{6.3}$-helical fold. Similar results have been obtained with many other gA mutants (Mazet et al., 1984; Durkin et al., 1990; Becker et al., 1991; Fonseca et al., 1992; Durkin et al., 1993; Jude et al., 1999), and the approach has been verified by solution NMR (Mattice et al., 1995; Sham et al., 2003).

Even though $\Delta\Delta G_f^{\ddagger} \approx 0$ kcal mol^{-1}, $\Delta\Delta G^0$ may be different from 0 kcal mol^{-1}. If $\Delta\Delta G^0$ is positive, there may be a strain at the subunit interface (Durkin et al., 1990, 1993); to relieve this strain the heterodimeric channels may switch between different conductance states (Durkin et al., 1993), and may even exhibit voltage-dependent transitions between closed and open channel states (Oiki et al., 1994, 1995).

In the case of gA and [D-Ala^2,Ser^3]gA, $\Delta\Delta G^0$ is positive ($\sim$0.25 kcal mol^{-1}) because the heterodimeric channel lifetimes (Fig. 2.9) are *less* than would be predicted from the lifetimes of the homodimeric channels (Fig. 2.2) in the absence of subunit-specific interactions: $\tau_{AB} \cdot \tau_{BA}/(\tau_{AA} \cdot \tau_{BB}) = 1$. The modest (relative) destabilization of the heterodimeric channels can be understood by examination of the gA channel structure. Because residue 3 in subunit A is in close proximity to residue 3 in subunit B (Fig. 2.10), the homodimeric [D-Ala^2,Ser^3]gA channels may be stabilized by hydrogen bond formation between the subunits—a bond that cannot be formed in the heterodimeric channels. The well-defined gA channel structure thus allows for quantitative studies on the interaction between amino acid residues at the channel/bilayer interface.

2.4 Channel Function

gA channels are water-filled pores that span lipid bilayers to catalyze selective ion movement across the membrane. The small pore radius restricts ions and water to move in single file through the pore (Levitt et al., 1978; Rosenberg and Finkelstein, 1978); but the rate of ion movement through the channels is large enough to allow for single-channel measurements to be done over a wide range of permeant ion concentrations and potentials (Hladky and Haydon, 1972; Neher et al., 1978; Andersen, 1983a; Cole et al., 2002). Because gA channels are seemingly ideally selective for monovalent cations (Myers and Haydon, 1972), single-channel measurements

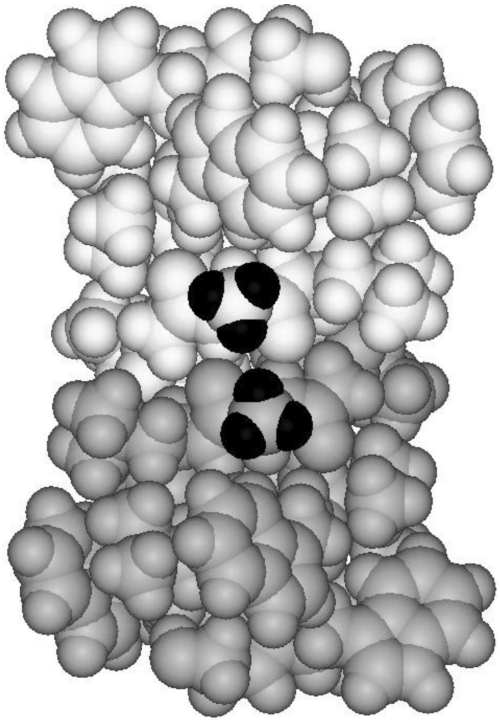

Fig. 2.10 Side view of the bilayer-spanning gramicidin A channel. The energy-minimized structure is the same as in Fig. 2.3, but turned 180° along the channel axis. The black atoms are the Ala^3 side-chain hydrogens on the respective subunits.

provide direct information about the net cation flux through the channel, meaning that it is possible to elucidate the kinetics of ion movement through the channel from current–concentration–voltage studies (see below). It is in this context important that: first, the $\beta^{6.3}$-helical channel conformation does not vary as function of the permeant ion type or concentration (Wallace et al., 1981; Katsaras et al., 1992; Tian and Cross, 1999); and second, the current through gA channels usually has little "excess" noise (cf. Fig. 2.1, where the SD of the current noise does not vary when a channel appears/disappears). These features should ensure that one indeed can relate function to the molecular structure and dynamics—and to use gA channels to critically evaluate computational strategies for understanding ion channel and, more generally, membrane protein function.

Before discussing the channels' permeability properties in detail, it is instructive to compare the measured conductances to the predictions of the simplest model of a water-filled pore, e.g., Hille (2001):

$$g_{\text{pred}} \approx \lambda^{\text{o}} \cdot C \cdot \frac{\pi \cdot r_{\text{p}}^2}{l_{\text{p}}}, \tag{2.10a}$$

where g_{pred} is the predicted single-channel conductance, λ^o the limiting equivalent conductivity, C the permeant ion concentration in the bulk aqueous phase, r_p the pore radius, and l_p the pore length. In this estimate, we neglect the access resistance to the channel (Hille, 1968; Läuger, 1976; Andersen, 1983c), which becomes important at low permeant ion concentrations (Andersen, 1983c).

For Na^+ permeation through gA channels ($\lambda^o_{Na} = 50.1$ S cm^2 mol^{-1} (Robinson and Stokes, 1959), 1.0 M NaCl, $r_p = 2$ Å and $l_p = 25$ Å), $g_{pred} \approx 250$ pS according to Eq. 2.10. Eq. 2.10 provides an overestimate, however; as noted by Ferry (1936), the relevant radius is not the geometric pore radius, but the difference between the pore and ion radius (r_i) because the ion centers are constrained to move within a relatively narrow column of radius $r_p - r_i$. Incorporating this geometric constraint, the "corrected" g_{pred} (g^{corr}_{pred}) becomes

$$g^{corr}_{pred} \approx \lambda^o \cdot C \cdot \frac{\pi \cdot (r_p - r_i)^2}{l_p}, \tag{2.10b}$$

and g^{corr}_{pred} (in 1.0 M NaCl) becomes ~70 pS ($r_{Na} \approx 0.95$ Å (Hille, 1975)). Because g^{corr}_{pred} is only fivefold higher than the measured conductance (Fig. 2.2), the channel cannot impose a major barrier for ion movement across the bilayer—a surprising result, given the significant electrostatic barrier associated with traversing the low dielectric constant bilayer hydrophobic core (Parsegian, 1969; Levitt, 1978). Even more surprising, in 1.0 M CsCl ($r_{Cs} \approx 1.63$ Å), $g^{corr}_{pred} \approx 13$ pS, which is almost fourfold less than the measured conductance of 50 pS. The channel has a *higher* conductance than the equivalent column of water!

That is, though gA channels are water-filled pores, they are not just water-filled pores. Even in the absence of a kinetic analysis of ion movement, one may conclude that favorable, short-range ion-channel interactions effectively compensate for the electrostatic barrier for ion movement through the low-dielectric bilayer core—such that the overall energetic barriers for ion movement are small (only a few $k_B T$).

2.4.1 Cation Binding in Gramicidin Channels

The low-dielectric bilayer hydrophobic core imposes a large electrostatic barrier for the transmembrane movement of alkali metal cations (Neumcke and Läuger, 1969; Parsegian, 1969).[1] Ion channels, and other membrane proteins, lower this barrier by

[1] The magnitude of this barrier can be estimated from the Born approximation for the free energy of transfer (ΔG^0_{trans}) for transferring an ion of valence z and radius r_i from a bulk phase of dielectric constant ε_1 to another bulk phase of dielectric constant ε_2 (Finkelstein and Cass, 1968; Parsegian, 1969):

$$\Delta G^0_{trans} \approx \frac{(ze_0)^2}{8 \cdot \pi \cdot r_i \cdot \varepsilon_0} \cdot \left(\frac{1}{\varepsilon_2} - \frac{1}{\varepsilon_1}\right),$$

where e_0 is the elementary charge and ε_0 is the permittivity of free space. The Born expression overestimates, cf. (Bockris and Reddy, 1970, Ch. 2), and provides only a rough estimate of the energies

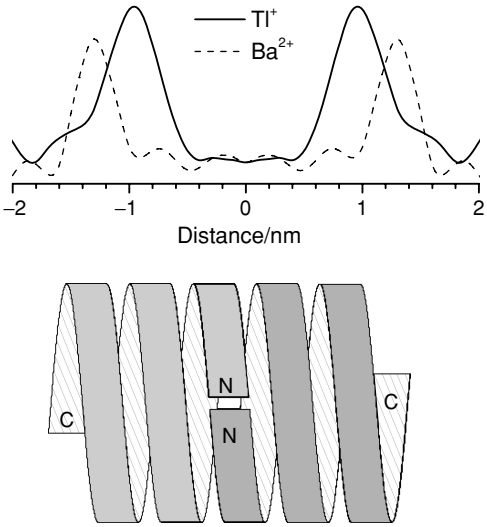

Fig. 2.11 Position of ion binding sites in gramicidin channels. Top: electron density profiles for Tl^+, with maxima at 9.6 ± 0.3 Å from the channel center (the maximum for K^+ is at the same position), and Ba^{2+}, with maxima at 13.0 ± 0.2 Å from the channel center. Redrawn after Olah et al. (1991). Bottom: schematic representation of the RH, SS $\beta^{6.3}$-helical dimer drawn on the same scale as the top panel.

providing a local environment with a higher dielectric constant (Parsegian, 1969; Levitt, 1978; Jordan, 1981), but the dielectric barrier is still $\sim$10 $k_B T$ (Jordan, 1981)—far too high to be compatible with the measured conductances. Efficient ion movement through gA channels depend on ion solvation by the pore-lining residues and the single file of pore water (Andersen and Procopio, 1980; Mackay et al., 1984; Allen et al., 2004a). Indeed, the free energies of transfer of small monovalent cations from water to formamide or dimethylformamide are negative, whereas they are positive for small monovalent anions (Cox et al., 1974). Not surprisingly, therefore, monovalent alkali metal cations bind with surprisingly high affinity to the channel and, even though there are no residues that form specific binding sites, the ions tend to be localized to delimited regions, or "binding sites." Fig. 2.11 shows the electron density profiles for Tl^+ and Ba^{2+} based on x-ray scattering experiments on gA incorporated into oriented DMPC multilayers (Olah et al., 1991).

For both Ba^{2+} and Tl^+, there are two major binding sites, with no significant ion occupancy outside these two sites. As would be expected from the Born expression (Footnote 2), the Ba^{2+} sites are located furthest away from the channel center, at the channel entrance; the Tl^+ sites are 3 Å deeper within the pore—within the

involved, $\sim 70\, k_B T$ for moving a monovalent ion of radius 1 Å from water ($\varepsilon = 80$) to a bulk hydrocarbon ($\varepsilon \approx 2$).

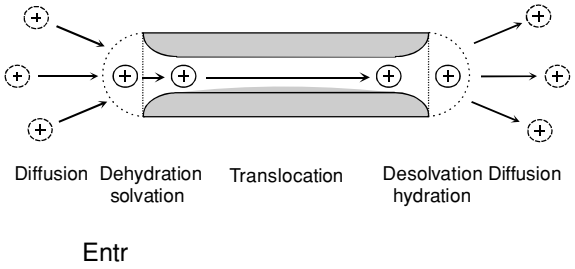

Fig. 2.12 The kinetic steps involved in ion movement through gA channels.

single-filing region. (The mono- and divalent cation binding sites also have been characterized by solution NMR on micelle-incorporated gA (Urry et al., 1982, 1989; Jing et al., 1995; Jing and Urry, 1995) solid-state NMR on gA in oriented DMPC bilayers (Tian and Cross, 1999). The results obtained with these different methods are in reasonable agreement.)

2.4.2 Discrete-State Kinetics of Channel-Catalyzed Ion Movement

Based on the preceding arguments, and the results in Fig. 2.11, ion movement through a gramicidin channel can be decomposed into the following steps (Fig. 2.12): ion entry—diffusion to channel entrance and association with the pore (dehydration and resolvation by polar groups in the pore wall); translocation through the channel interior; and ion exit—dissociation from the pore (desolvation/rehydration) and diffusion out into the other bulk solution.

This decomposition of the ion transfer into a series of discrete steps is an approximation because each step represents an electrodiffusive barrier crossing; yet it summarizes the essential features of channel-mediated ion permeation. Features that also can be deduced by inspection of the potential of mean force (PMF) for ion movement through the channels (see Section 2.5). Figure 2.12 thus serves as a convenient reference for the analysis of experiments on channels formed by gA and amino acid-substituted gA analogues.

Figure 2.11 shows the existence of two major ion binding "sites," with little occupancy outside of these sites, but not whether they are occupied simultaneously. It thus becomes necessary to consider a hierarchy of kinetic models when modeling ion movement through gramicidin channels. In the simplest case, the ion movement can be described in terms of transitions among three different states: 00, in which there is no ion in the pore; I0, in which there is an ion in the left "binding site"; and 0I, in which there is an ion in the right "binding site." Moreover, the transit time between these states is short compared to the residence times. In this case, the kinetic model for ion permeation becomes a three-barrier-two-site-one-ion (3B2S1I) model (Scheme III).

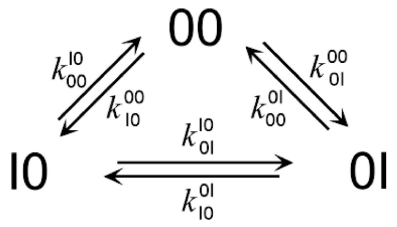

Scheme III

The (voltage-dependent) rate constants for the interconversions between the different states are denoted as $k_{\mathrm{ff}}^{\mathrm{ii}}$ (where the super- and subscripts denote the initial and final states, respectively), and the kinetic equations associated with Scheme III become:

$$\begin{aligned}
\frac{dW(00)}{dt} &= -\left(k_{10}^{00}\cdot[\mathrm{I}]_{\mathrm{l}} + k_{01}^{00}\cdot[\mathrm{I}]_{\mathrm{r}}\right)\cdot W(00) + k_{00}^{10}\cdot W(10) + k_{00}^{01}\cdot W(01)\\
\frac{dW(10)}{dt} &= -\left(k_{00}^{10} + k_{01}^{10}\right)\cdot W(10) + k_{10}^{00}\cdot[\mathrm{I}]_{\mathrm{l}}\cdot W(00) + k_{10}^{01}\cdot W(01)\\
\frac{dW(01)}{dt} &= -\left(k_{00}^{01} + k_{10}^{01}\right)\cdot W(01) + k_{01}^{00}\cdot[\mathrm{I}]_{\mathrm{r}}\cdot W(00) + k_{01}^{10}\cdot W(10)
\end{aligned} \tag{2.11}$$

subject to the conservation:

$$W(00) + W(10) + W(01) = 1, \tag{2.12}$$

where $W(00)$, etc., denotes the probability of being in the state 00, etc. In the steady state, which is of interest here,

$$\frac{W(00)}{dt} = \frac{W(10)}{dt} = \frac{W(01)}{dt} = 0 \tag{2.13}$$

and Eqs. 2.11–2.13 can be solved algebraically or by the graph-theoretical method of King and Altman (1956). The flux (j) through the channel is given by

$$\begin{aligned}
j &= k_{01}^{10}\cdot W(10) - k_{10}^{01}\cdot W(01)\\
&= \frac{k_{10}^{00}\cdot k_{01}^{10}\cdot k_{00}^{01}\cdot[\mathrm{I}]_{\mathrm{l}} - k_{01}^{00}\cdot k_{10}^{01}\cdot k_{00}^{10}\cdot[\mathrm{I}]_{\mathrm{r}}}{\mathrm{DD}},
\end{aligned} \tag{2.14}$$

where the flux from left to right is positive and DD is given by, cf. Andersen (1989)

$$\begin{aligned}
\mathrm{DD} = {} & k_{01}^{10}\cdot k_{00}^{01} + k_{10}^{01}\cdot k_{00}^{10} + k_{00}^{10}\cdot k_{00}^{01}\\
& + k_{10}^{00}\cdot[\mathrm{I}]_{\mathrm{l}}\cdot\left(k_{01}^{10} + k_{10}^{01} + k_{00}^{01}\right)\\
& + k_{01}^{00}\cdot[\mathrm{I}]_{\mathrm{r}}\cdot\left(k_{01}^{10} + k_{10}^{01} + k_{00}^{10}\right)
\end{aligned} \tag{2.15}$$

with the rate constants subject to the constraint imposed by detailed balance, e.g., Amdur and Hammes (1966), which for monovalent cation movement becomes:

$$\frac{k_{\mathrm{I0}}^{00} \cdot k_{\mathrm{0I}}^{\mathrm{I0}} \cdot k_{00}^{\mathrm{0I}}}{k_{\mathrm{0I}}^{00} \cdot k_{\mathrm{I0}}^{\mathrm{0I}} \cdot k_{00}^{\mathrm{I0}}} = \exp\left\{\frac{e_0 \cdot \Delta V}{k_{\mathrm{B}} T}\right\}, \tag{2.16}$$

where ΔV is the potential difference applied across the membrane ($\Delta V = V_{\mathrm{l}} - V_{\mathrm{r}}$).

Generally, the voltage dependence of the rate constants can be expressed as:

$$k_{\mathrm{ff}}^{\mathrm{ii}} = \kappa_{\mathrm{ff}}^{\mathrm{ii}} \cdot f_{\mathrm{ff}}^{\mathrm{ii}}(\Delta V), \tag{2.17}$$

where $\kappa_{\mathrm{ff}}^{\mathrm{ii}}$ denotes the 0 mV value for the rate constant in question, which can be determined from the PMF following Kramers (1940), see also Andersen (1989) and Roux et al. (2004), and $f_{\mathrm{ff}}^{\mathrm{ii}}(\Delta V)$ its voltage dependence. For an ion channel with equal permeant ion concentrations in the two aqueous phases, $[\mathrm{I}]_{\mathrm{l}} = [\mathrm{I}]_{\mathrm{r}} = [\mathrm{I}]$, there is no net flux at $\Delta V = 0$, and the detailed balance constraint, Eq. 2.16, can be expressed as

$$\frac{\kappa_{\mathrm{I0}}^{00} \cdot \kappa_{\mathrm{0I}}^{\mathrm{I0}} \cdot \kappa_{00}^{\mathrm{0I}}}{\kappa_{\mathrm{0I}}^{00} \cdot \kappa_{\mathrm{I0}}^{\mathrm{0I}} \cdot \kappa_{00}^{\mathrm{I0}}} = 1 \tag{2.18a}$$

and

$$\frac{f_{\mathrm{I0}}^{00}(\Delta V) \cdot f_{\mathrm{0I}}^{\mathrm{I0}}(\Delta V) \cdot f_{00}^{\mathrm{0I}}(\Delta V)}{f_{\mathrm{0I}}^{00}(\Delta V) \cdot f_{\mathrm{I0}}^{\mathrm{0I}}(\Delta V) \cdot f_{00}^{\mathrm{I0}}(\Delta V)} = \exp\left\{\frac{e_0 \cdot \Delta V}{k_{\mathrm{B}} T}\right\}. \tag{2.18b}$$

The single-channel current (i) is given by $e_0 \cdot j$,

$$i = e_0 \cdot \frac{k_{\mathrm{I0}}^{00} \cdot k_{\mathrm{0I}}^{\mathrm{I0}} \cdot k_{00}^{\mathrm{0I}} \cdot [\mathrm{I}]_{\mathrm{l}} - k_{\mathrm{0I}}^{00} \cdot k_{\mathrm{I0}}^{\mathrm{0I}} \cdot k_{00}^{\mathrm{I0}} \cdot [\mathrm{I}]_{\mathrm{r}}}{\mathrm{DD}}, \tag{2.19}$$

and the single-channel conductance (g) is given by $i/(\Delta V - E)$, where E is the equilibrium (or Nernst) potential for the ion, $E = (k_{\mathrm{B}} T/e_0) \cdot \ln\{[\mathrm{I}]_{\mathrm{l}}/[\mathrm{I}]_{\mathrm{r}}\}$ (where we disregard activity coefficient corrections).

In the limit $\Delta V \to 0$, and symmetric permeant concentrations, the single-channel conductance–concentration (g–C) relation becomes

$$g = \frac{g_{\max} \cdot [\mathrm{I}]}{K_{\mathrm{I}} + [\mathrm{I}]}. \tag{2.20}$$

For a symmetric channel ($\kappa_{\mathrm{I0}}^{00} = \kappa_{0\mathrm{I}}^{00}$, etc.), the expressions for $g_{\max}$ and K_{I} become

$$g_{\max} = \frac{e_0^2}{k_{\mathrm{B}}T} \cdot \frac{k_{0\mathrm{I}}^{\mathrm{I0}} \cdot k_{00}^{0\mathrm{I}}}{2 \cdot \left(2 \cdot k_{0\mathrm{I}}^{\mathrm{I0}} + k_{00}^{0\mathrm{I}}\right)} \tag{2.21a}$$

and

$$K_{\mathrm{I}} = \frac{k_{00}^{\mathrm{I0}}}{2 \cdot k_{\mathrm{I0}}^{00}}. \tag{2.21b}$$

Though Eq. 2.20 provides a satisfactory fit of the g–C relation for Na^+ through gA channels, with $K_{\mathrm{I}} = 0.20$ M and $g_{\max} = 15.8$ pS (Andersen et al., 1995), Scheme III does not provide a satisfactory description of the kinetics of Na^+ movement over an extended voltage range. More complex permeation models are called for.

Indeed, the two cation "binding sites" (Fig. 2.11) can be occupied simultaneously (Schagina et al., 1978), such that it becomes necessary to extend Scheme III to include also a kinetic state in which both sites are occupied (II). The minimal kinetic model for ion permeation thus becomes a three-barrier-two-site-two-ion (3B2S2I) model (Scheme IV):

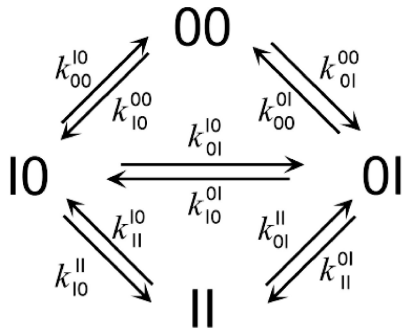

Scheme IV

The kinetic equations associated with Scheme IV can be solved algebraically, as above, but it usually is simpler to solve the equations associated with complex kinetic schemes using the King and Altman (1956) graph-theoretical approach, cf. Hille and Schwarz (1978). For a symmetric channel in the limit $V \rightarrow 0$, the g–C relation becomes (Heckmann, 1965; Urban et al., 1978; Finkelstein and Andersen, 1981):

$$g = \frac{e_0^2}{k_{\mathrm{B}}T} \cdot \frac{[\mathrm{I}]}{K_{\mathrm{I}} + [\mathrm{I}] + [\mathrm{I}]^2 / K_{\mathrm{II}}} \cdot \frac{\kappa_{0\mathrm{I}}^{\mathrm{I0}} \cdot \left(\kappa_{00}^{0\mathrm{I}} + \kappa_{\mathrm{II}}^{0\mathrm{I}} \cdot [\mathrm{I}]\right)}{2 \cdot \left(2 \cdot \kappa_{0\mathrm{I}}^{\mathrm{I0}} + \kappa_{00}^{0\mathrm{I}} + \kappa_{\mathrm{II}}^{0\mathrm{I}} \cdot [\mathrm{I}]\right)}, \tag{2.22}$$

where

$$K_{\mathsf{I}} = \frac{\kappa_{00}^{\mathsf{I0}}}{2 \cdot \kappa_{\mathsf{I0}}^{00}} \quad \text{and} \quad K_{\mathsf{II}} = \frac{2 \cdot \kappa_{0\mathsf{I}}^{\mathsf{II}}}{\kappa_{\mathsf{II}}^{0\mathsf{I}}} \tag{2.23}$$

(the factors of 2 arise because an ion can enter an empty channel, 00, and leave a double-occupied channel, II, from either side). The second term in Eq. 2.22 denotes the probability of finding the channel in a single-occupied state, $W(\mathsf{I0}) + W(0\mathsf{I})$, which reaches a maximum when $[\mathsf{I}] = \sqrt{K_{\mathsf{I}} \cdot K_{\mathsf{II}}}$; the third term keeps track of transitions in single-occupied channels, it reaches the limiting value $\kappa_{0\mathsf{I}}^{\mathsf{I0}}/4$ as $[\mathsf{I}] \to \infty$.

As evident by inspection of Eqs. 2.20–2.21 and Eqs. 2.22–2.23, *g–C* relations do not impart sufficient information (independent parameters) to allow for the determination of all the underlying rate constants in Schemes III and IV. For both schemes, however, it is possible to determine all the rate constants (and their associated voltage-dependent terms) from an analysis of the current–concentration–voltage (*i–C–V*) relations. In the case of Scheme IV, it even is possible to determine the 0 mV values for the rate constants by measuring the *g–C* relation and the correlation factor (f), which is defined as the ratio between the channel's equilibrium (or net) permeability coefficient (p_{I}) and the tracer permeability coefficient (p_{I}^*), cf. Heckmann (1972). The equilibrium and tracer permeability coefficients are given by (Finkelstein and Andersen, 1981; Andersen, 1989):

$$p_{\mathsf{I}} = \frac{k_{\mathrm{B}}T}{e_0^2} \cdot \frac{g}{[\mathsf{I}]} = \frac{1}{K_{\mathsf{I}} + [\mathsf{I}] + [\mathsf{I}]^2 / K_{\mathsf{II}}} \cdot \frac{\kappa_{0\mathsf{I}}^{\mathsf{I0}} \cdot \left(\kappa_{00}^{0\mathsf{I}} + \kappa_{\mathsf{II}}^{0\mathsf{I}} \cdot [\mathsf{I}]\right)}{2 \cdot \left(2 \cdot \kappa_{0\mathsf{I}}^{\mathsf{I0}} + \kappa_{00}^{0\mathsf{I}} + \kappa_{\mathsf{II}}^{0\mathsf{I}} \cdot [\mathsf{I}]\right)} \tag{2.24}$$

and

$$p_{\mathsf{I}}^* = \frac{1}{K_{\mathsf{I}} + [\mathsf{I}] + [\mathsf{I}]^2 / K_{\mathsf{II}}} \cdot \frac{\kappa_{0\mathsf{I}}^{\mathsf{I0}} \cdot \left(2 \cdot \kappa_{00}^{0\mathsf{I}} + \kappa_{\mathsf{II}}^{0\mathsf{I}} \cdot [\mathsf{I}]\right)}{2 \cdot \left(2 \cdot (2 \cdot \kappa_{0\mathsf{I}}^{\mathsf{I0}} + \kappa_{00}^{\mathsf{I0}}) + \kappa_{\mathsf{II}}^{0\mathsf{I}} \cdot [\mathsf{I}]\right)}, \tag{2.25}$$

such that the correlation factor becomes:

$$f = \frac{p_{\mathsf{I}}^*}{p_{\mathsf{I}}} = \frac{2 \cdot \kappa_{00}^{0\mathsf{I}} + \kappa_{\mathsf{II}}^{0\mathsf{I}} \cdot [\mathsf{I}]}{\kappa_{00}^{0\mathsf{I}} + \kappa_{\mathsf{II}}^{0\mathsf{I}} \cdot [\mathsf{I}]} \cdot \frac{2 \cdot \kappa_{0\mathsf{I}}^{\mathsf{I0}} + \kappa_{00}^{0\mathsf{I}} + \kappa_{\mathsf{II}}^{0\mathsf{I}} \cdot [\mathsf{I}]}{2 \cdot (2 \cdot \kappa_{0\mathsf{I}}^{\mathsf{I0}} + \kappa_{00}^{\mathsf{I0}}) + \kappa_{\mathsf{II}}^{0\mathsf{I}} \cdot [\mathsf{I}]}. \tag{2.26}$$

In single-occupied channels (Scheme III), $\kappa_{\mathsf{II}}^{0\mathsf{I}} = 0$ and $f \equiv 1$; that is, measuring the tracer permeability coefficient does not provide additional information. In double-occupied channels, $0.5 < f < 1$, and f approaches 1 as $[\mathsf{I}] \to 0$ or $[\mathsf{I}] \to \infty$. In this case there should be sufficient information to determine all the underlying rate constants—unless $\kappa_{0\mathsf{I}}^{\mathsf{I0}} < \kappa_{00}^{0\mathsf{I}}$ in which case $f \approx 1$.

Even Scheme IV needs to be enhanced, however, because the diffusional entry step (Fig. 2.12) constitutes a significant barrier to ion movement through gA channels (Andersen, 1983c). Diffusion limitation (DL) becomes important because

incoming ions must "hit" the pore entrance rather precisely—meaning that the channel is "hidden" behind a diffusion resistance. The existence of this diffusion limitation will complicate the mechanistic interpretation of structure–function studies because one may not be able to discern the "true" consequences of a sequence substitution. In addition to this complication, a potential difference applied across the bilayer (and channel) will change the interfacial ion concentrations. This interfacial polarization (IP) will in its own right have an impact on ion movement through the channel (Andersen, 1983b), which becomes increasingly important as the ionic strength (or permeant ion concentration) is reduced. When the 3B2S2I kinetic model is enhanced to incorporate both diffusion limitation and interfacial limitation, the resulting 3B2S2I(DL,IP) model provides an acceptable, discrete-state, kinetic description of ion permeation through gA channels (see Section 2.4.3).

2.4.3 Ion Permeation through gA Channels

The amino acid side chains do not contact the permeating ions, but the gA channels' permeability properties are modulated by amino acid substitutions throughout the sequence (Bamberg et al., 1976; Morrow et al., 1979; Heitz et al., 1982; Mazet et al., 1984; Russell et al., 1986; Koeppe et al., 1990): nonpolar→polar substitutions in the formyl-NH-terminal half of the sequence tend to reduce the conductance; polar→nonpolar substitutions in the carboxy-ethanolamide half tend to reduce the conductance. The primary mechanism by which amino acid substitutions alter the ion permeability appears to be electrostatic interactions between the permeating ions and the side chain dipoles (Mazet et al., 1984; Koeppe et al., 1990; Andersen et al., 1998; Busath et al., 1998).

The kinetics of ion movement through gA channels have been studied using single-channel measurements in glycerolmonoleate (Neher et al., 1978; Urban et al., 1980; Busath et al., 1998; Cole et al., 2002) or DPhPC (Becker et al., 1992) bilayers. Figures 2.13 and 2.14 show results obtained in DPhPC/*n*-decane with Na^+ as the permeant ion, as well as the fit of the 3B2S2I(DL,IP) model to the results.

The data span a large range of voltages and concentrations. One needs such a large data set to evaluate discrete-state kinetic models—as well as more detailed, physical descriptions of ion movement through a channel—because the $i - V$ relations are fairly linear. That is, the individual data points are highly correlated, such that the information content per point is limited. It is particularly important to have results at high potentials (at both low permeant ion concentrations, where the ion entry step is rate limiting, and high permeant concentrations, where ion exit becomes limiting).

When $[Na^+] \leq 0.1$ M or so, the i–V relations tend to level off toward a voltage-independent limit as V increases (Andersen, 1983c) because the rate of ion movement becomes determined by the voltage-independent diffusion step (Fig. 2.12). Yet, the unavoidable interfacial polarization causes the interfacial cation concentration to increase at the positive channel entrance (Andersen, 1983b), such that a bona fide voltage-independent limit is attained only in the limit where the ionic

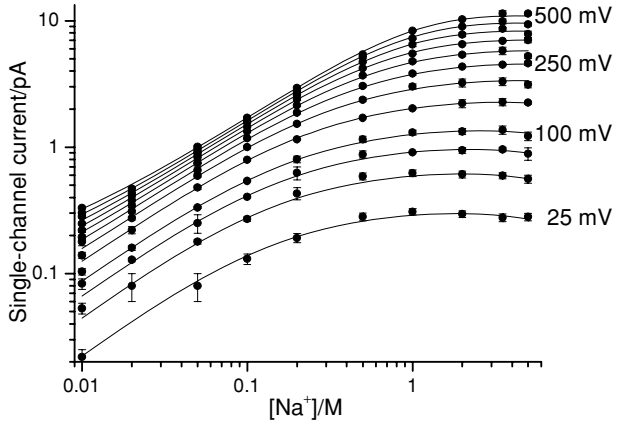

Figure 2.13 Current–voltage–concentration results for Na^+ moving through gA channels in DPhPC bilayers and fit of the 3B2S2I(DL,IP) model to the results (the rate constants are listed in Table 2.1). 25°C. O.S. Andersen and M.D. Becker, unpublished observations; from Andersen et al. (2005) with permission.

strength (adjusted using inert salt, which does not permeate through or block the channels) is much higher than the permeant cation concentration (Andersen, 1983b). This limiting current allows for the determination of the diffusion-limited ion access permeability (p_0), or rate constant (κ_0) (Hille, 1968; Hall, 1975; Läuger, 1976):

$$p_0 = 2\pi \cdot D_{\text{aq}} \cdot r_0 \tag{2.27a}$$

$$\kappa_0 = 2\pi \cdot D_{\text{aq}} \cdot r_0 \cdot N_{\text{A}}, \tag{2.27b}$$

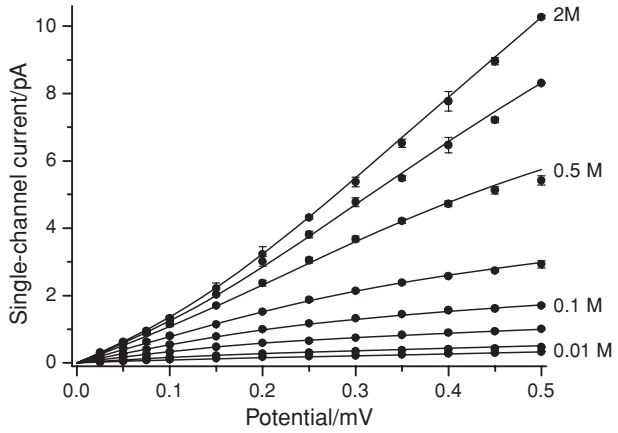

Figure 2.14 Current–voltage results for $[Na^+]$ between 0.01 and 2.0 M and fits of the 3B2S2I(DL,IP) model to the results. Results from Fig. 2.13; from Andersen et al. (2005) with permission.

where D_{aq} is the ion's diffusion coefficient and r_0 the channel's capture radius for the ion, which is equal to the difference between the effective pore and ion radii, cf. Eq. 2.10b and Ferry (1936), and N_A Avogadro's number. p_0 is $\sim 1.8 \times 10^{-13}$ $cm^3 \cdot s^{-1}$ for Na^+ and 3×10^{-13} $cm^3 \cdot s^{-1}$ for the higher alkali metal cations, corresponding to κ_0 being $\sim 10^8$ $M^{-1} \cdot s^{-1}$ for Na^+ and $\sim 2 \times 10^8$ $M^{-1} \cdot s^{-1}$ for the higher alkali metal cations (Andersen, 1983c). These values are comparable to diffusion-limited association rate constants in enzyme-catalyzed reactions (Eigen, 1974; Fersht, 1985). The diffusion-limited ion access permeability imposes an upper limit on the single-channel conductance (Hille, 1968; Läuger, 1976):

$$g_{lim} = \frac{e_0^2 \cdot p_0 \cdot [I]}{2 \cdot k_B T}, \tag{2.28}$$

which in the case of 0.1 M Na^+ is $\sim$34 pS—only about than sevenfold higher than the measured conductance (5.2 pS, Andersen, 1983a).

Assuming that the ion's diffusion coefficient adjacent to the pore entrance is equal to the bulk diffusion coefficient (which is questionable, see König et al., 1994), the channel's capture radius for the alkali metal cations is $\sim$0.3 Å (Andersen, 1983c). The small value of the capture radius provides for an estimate of an ion's thermal velocity (v_0), because the ions' overall collision rate with the pore entrance is $v_0 \cdot 2\pi \cdot r_0^2 \cdot C_0$, where C_0 is the ion concentration at the pore entrance. By contrast, the diffusion-limited rate of ion/channel encounters is $2\pi \cdot r_0 \cdot D \cdot (C_b - C_0)$, where C_b is the bulk ion concentration. When $r_0 > 1$ Å, as is the case for diffusion-limited reactions in bulk solutions, the diffusion-limited step is rate limiting. When $r_0 < 1$ Å, the relative resistance imposed by the collision step becomes increasingly important as r_0 decreases, which makes it possible to estimate v_0 to be $\sim 10^4$ cm s^{-1} (Andersen and Feldberg, 1996), as predicted by Einstein (1907).

When $[Na^+] > 1$ M, the channel usually is occupied by at least one Na^+, the slope of i–V relations increases as V increases (Fig. 2.13) because the rate of ion movement in this case becomes determined by voltage-dependent transitions within the pore (translocation and exit, Fig. 2.12) determine the overall rate of ion movement. That is, by examining the i–V–C relations over a large range of ion concentrations and applied potentials it is possible to "isolate" and explore the various steps in ion movement through the pore—and to determine the underlying rate constants. Table 2.1 summarizes results obtained with gA, as well as two Trp→Phe-substituted gA analogues [Phe^9]gA and [Phe^{15}]gA. These analogues form channels, structurally equivalent to gA channels, with conductances of 6 pS and 11 pS (in 1.0 M NaCl and 200 mV applied potential), respectively, as compared to 15 pS for gA channels (Becker et al., 1991).

Though it is possible to determine all the rate constants in the kinetic scheme, it is important to keep in mind what has been determined—rate constants. Attempts to convert a set of rate constants to a so-called energy profile are fraught with problems (Andersen and Koeppe, 1992; Andersen, 1999), and should be considered unnecessary obfuscation.

Table 2.1 Kinetics of Na^+ permeation through gA channels and Trp→Phe substituted gA channels

Trp→Phe substitution rate constant	None	Position 9	Position 15
κ_0 (M^{-1} $s^{-1}\times10^7$)	9	9	9
κ_{I0}^{00} (M^{-1} $s^{-1}\times10^7$)	41	51	7
κ_{00}^{I0} ($s^{-1}\times 10^7$)	11	26	4.6
κ_{0I}^{I0} ($s^{-1}\times 10^6$)	7	2.3	4.7
κ_{II}^{0I} (M^{-1} $s^{-1}\times 10^7$)	0.7	0.02	0.005
κ_{0I}^{II} ($s^{-1}\times10^7$)	2.8	0.3	0.02

DPhPC/*n*-decane bilayers; 25°C.

The rate constants, apart from κ_0, are defined in Scheme II and Eq. 2.5. The standard deviations, determined from Monte Carlo-based error analysis {Alper and Gelb, 1990}, are less than 20%, usually less then 10%. From Becker et al. {Becker, Koeppe, et al. 1992/d}.

Au: Pls. check if the units are identified correctly.

The predicted Na^+ affinities, and relative affinities for the first and second ion that binds, are listed in Table 2.2. Note that even though the *g–C* relation (determined in the limit $V\rightarrow0$) could be fitted quite well by Eq. 2.20, the deduced ion-channel dissociation constant (0.20 M) is higher than the dissociation deduced from the complete kinetic analysis. Also, the ratio $\kappa_{0I}^{I0}/\kappa_{00}^{I0}$ is less than 1, meaning that the correlation factor is close to 1.0. It is not possible to deduce all the rate constants in the kinetic scheme from the *g–C* relation and concentration dependence of the correlation factor.

To appreciate the channels' affinity for Na^+, it is useful to compare the Na^+ mole-fraction (n_{Na}) in the pore (n_{Na}^{pore}), which has ∼6 H_2O molecules in the single-filing stretch (Levitt et al., 1978; Rosenberg and Finkelstein, 1978; Allen et al., 2004a), to n_{Na} in the bulk solution (n_{Na}^{bulk}). At 0.14 M, $n_{Na}^{bulk}\approx 1/400$, whereas $n_{Na}^{pore}\approx 1/10$ (corresponding to a 5 M solution) or ∼40-fold higher than in the bulk solution. Na^+ therefore is preferentially solvated by the pore lining residues, as compared to the solvation in bulk water! A similar conclusion can be drawn for other ion-conducting channels (Andersen and Koeppe, 1992).

Table 2.2 Derived parameters for Na^+ permeation through gA and Trp→Phe substituted gA channels

Trp→Phe substitution parameter	None	Position 9	Position 15
K_I (M^{-1})	0.14	0.25	0.32
K_{II} (M^{-1})	8	38	13
K_{II}/K_I	58	150	39
$\kappa_{II}^{0I}/\kappa_{I0}^{00}$	0.02	0.004	0.007
$\kappa_{0I}^{II}/\kappa_{00}^{I0}$	0.25	0.01	0.007

The entries are calculated based on the parameters in Table 2.1, using a Monte Carlo-based error analysis, e.g. {Alper and Gelb, 1990}.

Au: Pls. check if the units are identified correctly.

2.4.4 Gramicidin Channels as Enzymes

Gramicidin channels, like other ion channels (and membrane proteins) catalyze ion movement across a lipid bilayer by providing a reaction path that obviates the ion's passage through the lipid bilayer hydrophobic core per se. Gramicidin channels therefore are enzymes, albeit members of a special class of enzymes in which no covalent bonds are made or broken during the catalytic cycle. It now is possible to estimate the channels' catalytic rate enhancement, the rate of channel-mediated ion movement (k_{cat}) relative to the rate noncatalyzed movement through the bilayer, k_{cat}/k_{non} (Wolfenden and Snider, 2001).

To a first approximation, k_{cat}/k_{non} can be equated with $K_{p/w}/K_{m/w}$, where $K_{p/w}$ and $K_{m/w}$ denote the ion partition coefficients into the pore and into the bilayer hydrophobic core, respectively, in the limit where the channel's ion occupancy is $\ll 1$. In this limit, one can determine $K_{p/w}$ from the preceding kinetic analysis: $K_{p/w} \approx n_{Na}^{pore}/n_{Na}^{bulk} \approx 10^2$. $K_{m/w}$ can be estimated to be $\sim 10^{-14}$ based on the conductance ($G_0 \approx 10^{-9}$ S cm^{-2}) of unmodified bilayers in 1.0 M NaCl (Hanai et al., 1965) using the relation (Hodgkin and Katz, 1949; Andersen, 1989):

$$G_0 = N_A \cdot \frac{(ze)^2}{k_B T} \cdot \frac{D_m}{d_0} \cdot K_{m/w} \cdot C, \tag{2.29}$$

where D_m is the ion's diffusion coefficient in the bilayer hydrophobic core ($\sim 10^{-5}$ cm^2·s^{-1}, cf. Schatzberg, 1965). We thus find that the catalytic rate enhancement is in the neighborhood of 10^{15} to 10^{16}, which is comparable to the rate enhancement observed for conventional enzymes (Wolfenden and Snider, 2001).

2.4.5 Ion–Ion Interactions May Be Water-Mediated

Tables 2.1 and 2.2 show that $K_{II}/K_I \gg 1$, indicative of repulsive ion–ion interactions; but the ratio differs among the channels, suggesting that ion–ion interactions within the doubly-occupied channels are not due solely to electrostatic interactions. This conclusion is supported by examining the ratios of association and dissociation rate constants for the first and the second ion entering (or leaving), the lower two lines in Table 2.2. Both ratios are decreased—with the major decrease being in the ratio of the association rate constants. This surprising result presumably means that the water in the pore (being relatively incompressible) plays an important role in mediating ion–ion interactions, see also Roux et al. (1995). It further suggests that the pore water needs to be considered in Brownian dynamics (BD) simulations of channel-catalyzed ion movement.

2.4.6 Importance of the Trp Residues for Ion Permeation

The four Trp residues at the pore entrance are important for both channel folding and channel function. They are oriented with their dipole moments directed away

from the channel center, the NH's toward the aqueous solution (Arseniev et al., 1986; Ketchem et al., 1997; Townsley et al., 2001), which will tend to lower the central electrostatic barrier below that estimated using a structure-less dielectric model (Jordan, 1984; Sancho and Martinez, 1991; Andersen et al., 1998).

Consistent with this idea, gA analogues with one or more Trp→Phe replacements form channels with decreased ion permeabilities (Becker et al., 1991), see Section 2.4.3. When all four Trp residues are replaced by Phe, the Cs^+ conductance is reduced sixfold (Heitz et al., 1982; Fonseca et al., 1992). The basis for the reduced conductance appears to be a greatly reduced rate constant for ion translocation through the channel, κ_{0l}^{l0}, as deduced by Becker et al. (1992) and Caywood et al. (2004), although the rate constant for ion entry also is reduced (Becker et al., 1992; Fonseca et al., 1992). The latter could arise because the amphipathic indoles may be able to move (a little) out beyond the hydrophobic membrane core, which could be important as an incoming ion sheds most of its hydration shell to become solvated by the peptide backbone. The backbone deformation that is needed to optimize ion–oxygen contacts (Noskov et al., 2004) will involve also side chain motions (Urry, 1973).

The changes in Na^+ permeation through single Trp→Phe substituted gramicidins have been examined in detail (Becker et al., 1992); see Tables 2.1 and 2.2. The kinetic analysis provides information about rate constants for ion translocation, but no information about the absolute barrier heights (or well depths) of the free energy profile for ion movement through the pore (Andersen, 1989, 1999). Such information can be extracted only through an appropriate physical theory, such as a hierarchical implementation of MD and BD simulations (Roux et al., 2004). Nevertheless, it is possible to estimate the *changes* in barrier heights and well depths as $k_B T \cdot \ln\{\kappa^{\text{Analogue}}/\kappa^{\text{Control}}\}$ for each of the transitions along the reaction coordinate (Andersen, 1989). We conclude that single Trp→Phe substitutions at the channel pore entrances (one in each subunit) may alter the barrier profile (decrease well depths, increase barrier heights) by several $k_B T$.

Trp→Phe substitutions increase the height of the central barrier. Because the sequence substitutions do not alter the structure of the subunit interface (Becker et al., 1991), the conductance changes most likely result from favorable electrostatic interactions between the indole dipole and the permeant ion (Andersen et al., 1998; Busath et al., 1998). Surprisingly, the sign of the Trp→Phe substitution-induced changes in the entry/exit barrier depends on the position where the substitution is made (Table 2.1), indicating that the side chain dynamics indeed are important for the rate of the ions' hydration/solvation.

2.4.7 Importance of the Lipid Bilayer

Changes in ion permeability as a result of amino acid substitutions are not surprising, even though the side chains do not contact the permeating ions. But only a detailed kinetic analysis would be able to reveal that the changes in the ion entry/exit kinetics depend on residue position. What *is* surprising is that even changes in the bilayer

Table 2.3 gA single-channel conductances in bilayers formed by phospholipids having different acyl chains

Phospholipid	Conductance (pS)
diphytanoyl-PC	15.0 ± 0.5
1-palmitoyl-2-oleoyl-PC*	11.3 ± 0.5
dioleoyl-PC*	13.0 ± 0.5
dilinoleoyl-PC*	14.9 ± 0.4

25°C, 1.0 M NaCl, 200 mV.
*Results from Girshman et al. {Girshman et al., 1997/d}.

lipid composition—the acyl chain composition—alter the channels' ion permeability (Table 2.3).

Even larger changes than those indicated in Table 2.3 can be observed when the polar head groups of the bilayer-forming lipids are varied. Moreover, the conductance is higher in bilayers formed by ether, as opposed to ester phospholipids (Providence et al., 1995), presumably because the interfacial dipole potential is less positive in bilayers formed by ether phospholipids (Gawrisch et al., 1992). It is important not to consider the lipid bilayer just to be some "inert" host for the channels of interest.

2.5 Molecular Dynamics Analysis of Ion Permeation

To obtain better insights into the molecular basis for channel (or membrane protein) function, it is necessary to establish direct links between the atomic structure of a channel (or protein) and its observed function. When establishing these links, it becomes important to consider explicitly that channel proteins (as well as the water in the pore) are composed of discrete atoms that constantly undergo thermal fluctuations, from the rapid (picosecond) vibrations, through slower (multi-nanosecond) global reorientations and side-chain isomerizations, to long timescale (microsecond to second) conformational changes (Karplus and McCammon, 1981). The energetic consequences of these fluctuations are illustrated in Fig. 2.15, which shows fluctuations in potential energy for a K^+ in a gA channel imbedded in a dimyristoylphosphatidylcholine bilayer.

The fluctuations in energy are large because the pore is narrow, meaning that even small variations in the ion–carbonyl distance become important (Allen et al., 2004b). It is important to consider them when constructing permeation models.

Though MD simulations, in principle, should provide the desired tool for incorporating molecular reality and the consequences of molecular flexibility into descriptions of channel-mediated ion movement (Edwards et al., 2002), one cannot reach the necessary level of insight through "brute force" MD simulations (Roux, 2002; Roux et al., 2004), because the measured ion flux typically corresponds to ion transit times of ~100 ns—much longer than typical MD trajectories (Roux, 2002). Indeed, when using MD simulations to predict the PMF for ion movement through

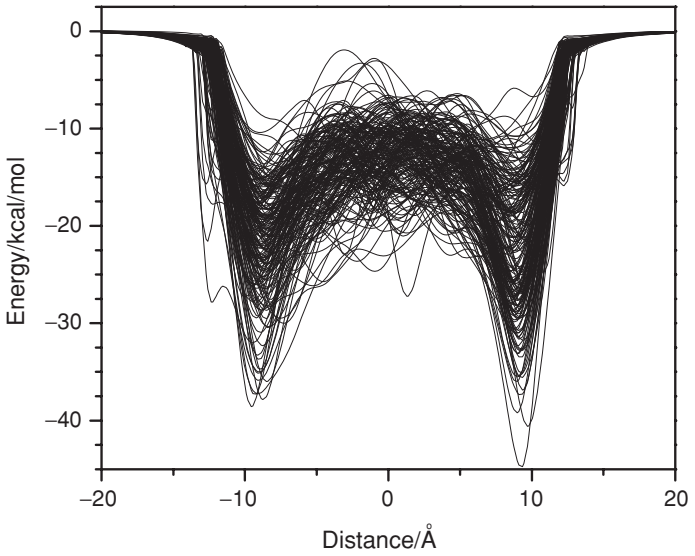

Figure 2.15 Small, Angstrom-scale thermal fluctuations in the gA structure produce large variations in the energetics of ion permeation, when used in models based on any one rigid structure. The figure shows Poisson solutions for 194 frames from a 4 ns MD trajectory initiated with the PDB:1JNO gA structure, and using a 1.4 Å water probe to define the high-dielectric constant region in the pore. Each sample was oriented such that the channel axis coincides, as closely as possible, with the fixed z-axis of the system. Distance is measured from the channel center. The variations in the potential profile are as much as 39 kcal mol^{-1}. After Allen et al. (2004b).

gA channels, the barrier heights are too high by many kcal mol^{-1} (Roux and Karplus, 1993; Allen et al., 2003), meaning that the predicted conductances are several orders of magnitude less than those observed experimentally. This is of concern because the small and relatively well-behaved gA channels should be particularly amenable to in-depth theoretical analysis and computer simulations.

There is reason for optimism, nevertheless. Fig. 2.16 shows two recently determined PMFs (free energy profiles) for K^+ permeation through gA channels (Allen et al., 2004a).

The main structural features of the PMFs, i.e., two cation binding sites near the channel's end separated by a central barrier, are qualitatively consistent with Fig. 2.11 which has been deduced from experiments (Urry et al., 1989; Olah et al., 1991). From a quantitative point of view, however, the "uncorrected" PMF in Fig. 2.16 continues to display a central barrier that is markedly too high, a problem similar to what has been observed in previous studies and which must be addressed and resolved.

After correcting for two potentially serious artifacts, the resulting "corrected" PMF in Fig. 2.16 leads to predicted experimental observables that are in semiquantitative agreement with experimental results. The first artifact is introduced by the periodic boundary conditions of the finite simulation system, which cause a spurious

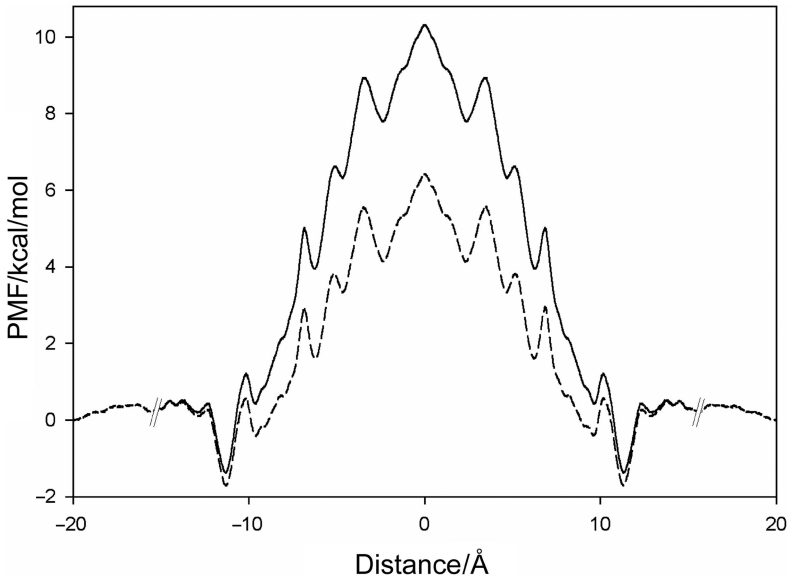

Figure 2.16 One-dimensional PMF, or free energy profile, for K^+ along the gA axis. The upper solid curve denotes the initial result of MD simulations. The free energy profile is not meaningful beyond the cuts at $z = \pm 15$ Å because no absolute reference of such a one-dimensional PM can be defined for large z (Roux et al., 2004). The lower dashed curve denotes the PMF corrected for size, and membrane dielectric constant (see text). After Allen et al. (2004a); modified from Andersen et al. (2005) with permission.

destabilization of the permeating ion in the channel relative to the bulk, which disappears if the system becomes exceedingly large (Hünenberger and McCammon, 1999). The second artifact arises because the hydrocarbon chains of the lipids are not polarizable in MD force fields, such that this region is treated as corresponding to a dielectric constant of 1, whereas it should be ∼2 (Huang and Levitt, 1977; Simon and McIntosh, 1986; Åqvist and Warshel, 1989), i.e., the dielectric constant of bulk hydrocarbons (Smyth, 1955), or even higher (Mamanov et al., 2003).

It is possible to correct for these artifactual contributions to the energy profile by a continuum electrostatic approximation using the configurations of the MD trajectories to average over protein and single-file water configurations (Allen et al., 2004a). It thus turns out that the periodic boundary conditions cause the ion of interest to interact with phantom charges in the infinite array of channels in the simulation system, which causes a spurious energy barrier on the order of 2 kcal mol^{-1} when the ion is in the middle of the channel. Moreover, a change of dielectric constant for the bilayer core from 1 to 2 stabilizes the ion in the channel by about 2 kcal mol^{-1} (Allen et al., 2006). The barrier in the corrected PMF in Fig. 2.16 therefore is about 4 kcal mol^{-1} lower than in the original PMF, which in a single ion occupied channel permeation model (Scheme III) corresponds to a 1000-fold increase in the predicted ion permeability. Indeed, the maximal conductance for K^+ (again assuming single

ion occupancy) is predicted to be ∼0.8 pS—"only" 30-fold less than the measured value of ∼25 pS in 1.0–2.0 M KCl and diphytanoylphosphatidylcholine bilayers (Andersen, 1983a; Bingham et al., 2003).

Some problems persist because the location and depth of the predicted binding sites differ somewhat from the experimental values (Urry et al., 1989; Olah et al., 1991): the binding sites are too far from the channel center and too shallow to be compatible with the observed ion affinities; but the predicted single-ion dissociation constant ($K_I \approx 0.34$ M) differs only by a factor five from the one predicted from the kinetic analysis of i–V–C results in gA channels ($K_I \approx 0.07$ M, O.S. Andersen and M.D. Becker, unpublished results). Both problems are likely to result from the use of nonpolarizable force fields to evaluate the ion–peptide backbone interactions, which therefore will tend to be underestimated. Another problem, which has not been fully resolved, is that the water models used in MD have been developed to describe bulk solution properties, which may differ from those of the single-file column of water in the channel pore. Because the PMF effectively arises as the sum of contributions from the permeating ion's interaction with the channel peptide, the single-filing water in the pore, and the bilayer hydrophobic core (Allen et al., 2004a), both the position and depth of the energy minima are likely to be particularly sensitive to the choice of force fields.

Given the progress that is taking place in terms of developing force fields that include induced polarization (Lamoureux and Roux, 2003; Lamoureux et al., 2003; Anisimov et al., 2004), there is every reason to be optimistic about the future. Indeed, even the present generation of force fields predicts changes in the central barrier (which should reflect primarily long-range electrostatic interactions) that are in near-quantitative agreement with experimental results (Allen et al., 2006), which suggests that one with some confidence can begin to use MD to understand the basis for amino acid substitution-induced *changes* in channel function.

2.6 Conclusion

The gramicidin channels possess remarkably well-defined structural and functional features that allow for detailed insights into the molecular basis for channel function. The channel's permeability properties can be modulated by changes in the amino acid sequence and the channels' bilayer environment. Single amino acid substitutions do not induce major changes in channel structure. It is difficult, however, to exclude that "minor" changes in side chain orientation or dynamics could be important for the observed changes in ion permeability. It is in this context important that the modest channel size allows for detailed computational analysis, which promises to provide atomic-level insights into the microphysics underlying ion permeation. This combination of features remains unprecedented, and suggests that the gA channels will become increasingly important as test beds for developing theoretical models of channel-catalyzed ion permeation and to critically evaluate (and improve) atomistic simulations of ion permeability.

Acknowledgments

This work was supported in part by the NIH under grants GM21342 (OSA), RR15569 (REK), GM62342 (BR), and GM70971 (OSA, REK and BR). We thank T. W. Allen, M. D. Becker, A. E. Daily, D. V. Greathouse, E. A. Hobart, H. Ingolfsson, T. Olson, S. Shobana, and S. E. Tape for stimulating discussions, technical assistance, and comments on the manuscript.

References

Abdul-Manan, N., and J.F. Hinton. 1994. Conformational states of gramicidin A along the pathway to the formation of channels in model membranes determined by 2D NMR and circular dichroism spectroscopy. *Biochemistry* 33:6773–6783.

Allen, T.W., O.S. Andersen, and B. Roux. 2003. The structure of gramicidin A in a lipid bilayer environment determined using molecular dynamics simulations and solid-state NMR data. *J. Am. Chem. Soc.* 125:9868–9878.

Allen, T.W., O.S. Andersen, and B. Roux. 2004a. Energetics of ion conduction through the gramicidin channel. *Proc. Natl. Acad. Sci. USA* 101:117–122.

Allen, T.W., O.S. Andersen, and B. Roux. 2004b. On the importance of atomic fluctuations, protein flexibility and solvent in ion permeation. *J. Gen. Physiol.* 124:679–690.

Au: Please update this reference.

Allen, T.W., O.S. Andersen, and B. Roux. 2006. Ion permeation through a narrow channel: Using gramicidin to ascertain all-atom molecular dynamics potential of mean force methodology and biomolecular force fields. *Biophys. J.* 90: under revision.

Allen, T.W., T. Bastug, S. Kuyucak, and S.-H. Chung. 2003. Gramicidin A channel as a test ground for molecular dynamics force fields. *Biophys. J.* 84:2159.

Amdur, I., and G.G. Hammes. 1966. Chemical Kinetics: Principles and Selected Topics. McGraw-Hill, New York.

Andersen, O.S. 1983a. Ion movement through gramicidin A channels. Single-channel measurements at very high potentials. *Biophys. J.* 41:119–133.

Andersen, O.S. 1983b. Ion movement through gramicidin A channels. Interfacial polarization effects on single-channel current measurements. *Biophys. J.* 41:135–146.

Andersen, O.S. 1983c. Ion movement through gramicidin A channels. Studies on the diffusion-controlled association step. *Biophys. J.* 41:147–165.

Andersen, O.S. 1989. Kinetics of ion movement mediated by carriers and channels. *Methods Enzymol.* 171:62–112.

Andersen, O.S. 1999. Graphic representation of the results of kinetic analyses. *J. Gen. Physiol.* 114:589–590.

Andersen, O.S., H.-J. Apell, E. Bamberg, D.D. Busath, R.E. Koeppe II, F.J. Sigworth, G. Szabo, D.W. Urry, and A. Woolley. 1999. Gramicidin channel controversy—the structure in a lipid environment. *Nat. Struct. Biol.* 6:609.

Andersen, O.S., and S.W. Feldberg. 1996. The heterogeneous collision velocity for hydrated ions in aqueous solutions is $\sim 10^4$ cm/s. *J. Phys. Chem.* 100:4622–4629.

Andersen, O.S., D.V. Greathouse, L.L. Providence, M.D. Becker, and R.E. Koeppe II. 1998. Importance of tryptophan dipoles for protein function: 5-fluorination of tryptophans in gramicidin A channels. *J. Am. Chem. Soc.* 120:5142–5146.

Andersen, O.S., and R.E. Koeppe II. 1992. Molecular determinants of channel function. *Physiol. Rev.* 72:S89–S158.

Andersen, O.S., R.E. Koeppe II, and B. Roux. 2005. Gramicidin channels. *IEEE Trans. Nanobioscience* 4:10–20.

Andersen, O.S., J.A. Lundbæk, and J. Girshman. 1995. Channel function and channel-lipid bilayer interactions. *In*: Dynamical Phenomena in Living Systems. E. Mosekilde and O.G. Mouritsen, editors. Springer, New York, pp. 131–151.

Andersen, O.S., and J. Procopio. 1980. Ion movement through gramicidin A channels. On the importance of the aqueous diffusion resistance and ion–water interactions. *Acta Physiol. Scand.; Suppl.* 481:27–35.

Andersen, O.S., G. Saberwal, D.V. Greathouse, and R.E. Koeppe II. 1996. Gramicidin channels—a solvable membrane "protein" folding problem. *Ind. J. Biochem. Biophys.* 33:331–342.

Anisimov, V.M., I.V. Vorobyov, G. Lamoureux, S. Noskov, B. Roux, and A.D. MacKerell Jr. 2004. CHARMM all-atom polarizable force field parameter development for nucleic acids. *Biophys. J.* 86:415a.

Åqvist, J., and A. Warshel. 1989. Energetics of ion permeation through membrane channels. Solvation of Na^+ by gramicidin A. *Biophys. J.* 56:171–182.

Arseniev, A.S., A.L. Lomize, I.L. Barsukov, and V.F. Bystrov. 1986. Gramicidin A transmembrane ion-channel. Three-dimensional structure reconstruction based on NMR spectroscopy and energy refinement. *Biol. Membr.* 3:1077–1104.

Bamberg, E., H.J. Apell, and H. Alpes. 1977. Structure of the gramicidin A channel: Discrimination between the $\pi_{L,D}$ and the β helix by electrical measurements with lipid bilayer membranes. *Proc. Natl. Acad. Sci. USA* 74:2402–2406.

Bamberg, E., H.J. Apell, H. Alpes, E. Gross, J.L. Morell, J.F. Harbaugh, K. Janko, and P. Läuger. 1978. Ion channels formed by chemical analogs of gramicidin A. *Fed. Proc.* 37:2633–2638.

Bamberg, E., and P. Läuger. 1973. Channel formation kinetics of gramicidin A in lipid bilayer membranes. *J. Membr. Biol.* 11:177–194.

Bamberg, E., K. Noda, E. Gross, and P. Läuger. 1976. Single-channel parameters of gramicidin A, B, and C. *Biochim. Biophys. Acta* 419:223–228.

Bass, R.B., P. Strop, M. Barclay, and D.C. Rees. 2002. Crystal structure of *Escherichia coli* MscS, a voltage-modulated and mechanosensitive channel. *Science* 298:1582–1587.

Becker, M.D., D.V. Greathouse, R.E. Koeppe II, and O.S. Andersen. 1991. Amino acid sequence modulation of gramicidin channel function. Effects of

tryptophan-to-phenylalanine substitutions on the single-channel conductance and duration. *Biochemistry* 30:8830–8839.

Becker, M.D., R.E. Koeppe II, and O.S. Andersen. 1992. Amino acid substitutions and ion channel function: Model-dependent conclusions. *Biophys. J.* 62:25–27.

Bingham, N.C., N.E. Smith, T.A. Cross, and D.D. Busath. 2003. Molecular dynamics simulations of Trp side-chain conformational flexibility in the gramicidin A channel. *Biopolymers* 71:593–600.

Bockris, J.O'.M., and A.K.N. Reddy. 1970. Modern Electrochemistry, Vol. 1. Plenum, New York.

Burkhart, B.M., N. Li, D.A. Langs, W.A. Pangborn, and W.L. Duax. 1998. The conducting form of gramicidin A is a right-handed double-stranded double helix. *Proc. Natl. Acad. Sci. USA* 95:12950–12955.

Busath, D.D. 1993. The use of physical methods in determining gramicidin channel structure and function. *Annu. Rev. Physiol.* 55:473–501.

Busath, D.D., O.S. Andersen, and R.E. Koeppe II. 1987. On the conductance heterogeneity in membrane channels formed by gramicidin A. A cooperative study. *Biophys. J.* 51:79–88.

Busath, D.D., and G. Szabo. 1981. Gramicidin forms multi-state rectifying channels. *Nature* 294:371–373.

Busath, D.D., C.D. Thulin, R.W. Hendershot, L.R. Phillips, P. Maughan, C.D. Cole, N.C. Bingham, S. Morrison, L.C. Baird, R.J. Hendershot, M. Cotten, and T.A. Cross. 1998. Noncontact dipole effects on channel permeation. I. Experiments with (5F-indole)Trp^{13} gramicidin A channels. *Biophys. J.* 75:2830–2844.

Bystrov, V.F., and A.S. Arseniev. 1988. Diversity of the gramicidin A spatial structure: Two-dimensional proton NMR study in solution. *Tetrahedron* 44:925–940.

Caywood, D., J. Durrant, P. Morrison, and D.D. Busath. 2004. The Trp potential deduced from gramicidin A/gramicidin M channels. *Biophys. J.* 86:55a.

Chang, G., R.H. Spencer, A.T. Lee, M.T. Barclay, and D.C. Rees. 1998. Structure of the MscL homolog from *Mycobacterium tuberculosis*: A gated mechanosensitive ion channel. *Science* 282:2220–2226.

Cifu, A.S., R.E. Koeppe II, and O.S. Andersen. 1992. On the supramolecular structure of gramicidin channels. The elementary conducting unit is a dimer. *Biophys. J.* 61:189–203.

Cole, C.D., A.S. Frost, N. Thompson, M. Cotten, T.A. Cross, and D.D. Busath. 2002. Noncontact dipole effects on channel permeation. VI. 5F- and 6F-Trp gramicidin channel currents. *Biophys. J.* 83:1974–1986.

Cornell, B.A., F. Separovic, A.J. Baldassi, and R. Smith. 1988. Conformation and orientation of gramicidin A in oriented phospholipid bilayers measured by solid state carbon-13 NMR. *Biophys. J.* 53:67–76.

Cornell, B.A., F. Separovic, D.E. Thomas, A.R. Atkins, and R. Smith. 1989. Effect of acyl chain length on the structure and motion of gramicidin A in lipid bilayers. *Biochim. Biophys. Acta* 985:229–232.

Cowan, S.W., and J.P. Rosenbusch. 1994. Folding pattern diversity of integral membrane proteins. *Science* 264:914–916.

Cowan, S.W., T. Schirmer, G. Rummel, M. Steiert, R. Ghosh, R.A. Pauptit, J.N. Jansonius, and J.P. Rosenbusch. 1992. Crystal structures explain functional properties of two *E. coli* porins. *Nature* 358:727–733.

Cox, B.G., G.R. Hedwig, A.J. Parker, and D.W. Watts. 1974. Solvation of ions. XIX Thermodynamic properties for transfer of single ions between protic and dipolar aprotic solvents. *Aust. J. Chem.* 27:477–501.

Cross, T.A. 1994. Structural biology of peptides and proteins in synthetic membrane environments by solid-state NMR spectroscopy. *Annu. Rep. NMR Spetrosc.* 29:123–167.

Cross, T.A., A. Arseniev, B.A. Cornell, J.H. Davis, J.A. Killian, R.E. Koeppe II, L.K. Nicholson, F. Separovic, and B.A. Wallace. 1999. Gramicidin channel controversy-revisited. *Nat. Struct. Biol.* 6:610–611; discussion 611–612.

Davis, J.H., and M. Auger. 1999. Static and magic angle spinning NMR of membrane peptides and proteins. *Progr. Nucl. Mag. Res. Spectr.* 35:1–84.

Dill, K.A. 1990. Dominant forces in protein folding. *Biochemistry* 29:7133–7155.

Dill, K.A., T.M. Truskett, V. Vlachy, and B. Hribar-Lee. 2005. Modeling water, the hydrophobic effect, and ion solvation. *Annu. Rev. Biophys. Biomol. Struct.* 34:173–199.

Doyle, D.A., J. Morais Cabral, R.A. Pfuetzner, A. Kuo, J.M. Gulbis, S.L. Cohen, B.T. Chait, and R. MacKinnon. 1998. The structure of the potassium channel: Molecular basis of K^+ conduction and selectivity. *Science* 280:69–77.

Dubos, R.J. 1939. Studies on a bactericidal agent extracted from a soil bacillus I. Preparation of the agent. Its activity*in vitro*. *J. Exp. Med.* 70:1–10.

Durkin, J.T., R.E. Koeppe II, and O.S. Andersen. 1990. Energetics of gramicidin hybrid channel formation as a test for structural equivalence. Side-chain substitutions in the native sequence. *J. Mol. Biol.* 211:221–234.

Durkin, J.T., L.L. Providence, R.E. Koeppe II, and O.S. Andersen. 1992. Formation of non-β-helical gramicidin channels between sequence-substituted gramicidin analogues. *Biophys. J.* 62:145–159.

Durkin, J.T., L.L. Providence, R.E. Koeppe II, and O.S. Andersen. 1993. Energetics of heterodimer formation among gramicidin analogues with an NH_2-terminal addition or deletion. Consequences of a missing residue at the join in channel. *J. Mol. Biol.* 231:1102–1121.

Edwards, S., B. Corry, S. Kuyucak, and S.-H. Chung. 2002. Continuum electrostatics fails to describe ion permeation in the gramicidin channel. *Biophys. J.* 83:1348.

Eigen, M. 1974. Diffusion control in biochemical reactions. *Quant. Stat. Mech. Nat. Sci.* 37–61.

Einstein, A. 1907. Theoretische Betrachtungen über der Brownsche Bewegungen. *Zeit. f. Elektrochemie* 13:41–42.

Engelman, D.M., T.A. Steitz, and A. Goldman. 1986. Identifying nonpolar transbilayer helices in amino acid sequences of membrane proteins. *Annu. Rev. Biophys. Biophys. Chem.* 15:321–353.

Evans, E.A., and R.M. Hochmuth. 1978. Mechanochemical properties of membranes. *Curr. Top. Membr. Transp.* 10:1–64.

Au: Please provide the volume number, if any.

Ferry, J.D. 1936. Statistical evaluation of sieve constants in ultrafiltration. *J. Gen Physiol.* 20:95–104.

Fersht, A. 1985. Enzyme Structure and Mechanism, 2nd Ed.

Finkelstein, A. 1974. Aqueous pores created in thin lipid membranes by the antibiotics nystatin, amphotericin B and gramicidin A. Implications for pores in plasma membranes. *In*: Drugs and Transport Processes. B.A. Callingham, editor. MacMillan, London, pp. 241–250.

Finkelstein, A., and O.S. Andersen. 1981. The gramicidin A channel: A review of its permeability characteristics with special reference to the single-file aspect of transport. *J. Membr. Biol.* 59:155–171.

Finkelstein, A., and A. Cass. 1968. Permeability and electrical properties of thin lipid membranes. *J. Gen. Physiol.* 52:145s–172s.

Fonseca, V., P. Daumas, L. Ranjalahy-Rasoloarijao, F. Heitz, R. Lazaro, Y. Trudelle, and O.S. Andersen. 1992. Gramicidin channels that have no tryptophan residues. *Biochemistry* 31:5340–5350.

Galbraith, T.P., and B.A. Wallace. 1998. Phospholipid chain length alters the equilibrium between pore and channel forms of gramicidin. *Faraday Discuss.* 159–164; discussion 225–246.

Gawrisch, K., D. Ruston, J. Zimmerberg, V.A. Parsegian, R.P. Rand, and N. Fuller. 1992. Membrane dipole potentials, hydration forces, and the ordering of water at membrane surfaces. *Biophys. J.* 61:1213–1223.

Gekko, K., and H. Noguchi. 1979. Compressibility of globular proteins in water at 25 °C. *J. Phys. Chem.* 83:2706–2714.

Greathouse, D.V., J.F. Hinton, K.S. Kim, and R.E. Koeppe II. 1994. Gramicidin A/short-chain phospholipid dispersions: Chain length dependence of gramicidin conformation and lipid organization. *Biochemistry* 33:4291–4299.

Greathouse, D.V., R.E. Koeppe II, L.L. Providence, S. Shobana, and O.S. Andersen. 1999. Design and characterization of gramicidin channels. *Methods Enzymol.* 294:525–550.

Gruner, S.M. 1985. Intrinsic curvature hypothesis for biomembrane lipid composition: A role for nonbilayer lipids. *Proc. Natl. Acad. Sci. USA* 82:3665–3669.

Hall, J.E. 1975. Access resistence of a small circular hole. *J. Gen. Physiol.* 66:531–532.

Hanai, T., D.A. Haydon, and J. Taylor. 1965. The variation of capacitance and conductance of bimolecular lipid membranes with area. *J. Theor. Biol.* 9:433–443.

Harold, F.M., and J.R. Baarda. 1967. Gramicidin, valinomycin, and cation permeability of *Streptococcus faecalis*. *J. Bacteriol.* 94:53–60.

He, K., S.J. Ludtke, Y. Wu, H.W. Huang, O.S. Andersen, D. Greathouse, and R.E. Koeppe II. 1994. Closed state of gramicidin channel detected by X-ray in-plane scattering. *Biophys. Chem.* 49:83–89.

Heckmann, K. 1965. Zur Theorie der "single file" diffusion. I. *Z. Phys. Chem. N.F.* 44:184–203.

Heckmann, K. 1972. Single file diffusion. *Biomembranes* 3:127–153.

Au: Please provide the name of the publisher and its location.

Au: Please provide the volume number, if any.

Heitz, F., G. Spach, and Y. Trudelle. 1982. Single channels of 9,11,13,15-destryptophyl-phenylalanyl-gramicidin A. *Biophys. J.* 40:87–89.

Herrell, W.E., and D. Heilman. 1941. Experimental and clinical studies on gramicidin. *J. Clin. Invest.* 20:583–591.

Hille, B. 1968. Pharmacological modifications of the sodium channels of frog nerve. *J. Gen. Physiol.* 51:199–219.

Hille, B. 1975. Ionic selectivity of Na and K channels in nerve membranes. *Membranes* 3:255–323.

Hille, B. 2001. Ionic Channels of Excitable Membranes, 3rd Ed. Sinauer, Sunderland, MA.

Hille, B., and W. Schwarz. 1978. Potassium channels as multi-ion single-file pores. *J. Gen. Physiol.* 72:159–162.

Hladky, S.B., and D.A. Haydon. 1970. Discreteness of conductance change in bimolecular lipid membranes in the presence of certain antibiotics. *Nature* 225:451–453.

Hladky, S.B., and D.A. Haydon. 1972. Ion transfer across lipid membranes in the presence of gramicidin A. I. Studies of the unit conductance channel. *Biochim. Biophys. Acta* 274:294–312.

Hodgkin, A.L., and B. Katz. 1949. The effect of sodium ions on the electrical activity of the giant axon of the squid. *J. Physiol.* 108:37–77.

Hotchkiss, R.D. 1944. Gramicidin, tyrocidine, and tyrothricin. *Adv. Enzymol.* 4:153–199.

Hu, W., and T.A. Cross. 1995. Tryptophan hydrogen bonding and electric dipole moments: Functional roles in the gramicidin channel and implications for membrane proteins. *Biochemistry* 34:14147–14155.

Huang, H.W. 1986. Deformation free energy of bilayer membrane and its effect on gramicidin channel lifetime. *Biophys. J.* 50:1061–1070.

Huang, W., and D.G. Levitt. 1977. Theoretical calculation of the dielectric constant of a bilayer membrane. *Biophys. J.* 17:111–128.

Hünenberger, P.H., and J.A. McCammon. 1999. Ewald artifacts in computer simulations of ionic solvation and ion–ion interaction: A continuum electrostatics study. *J. Chem. Phys.* 110:1856.

Jagannadham, M.V., and R. Nagaraj. 2005. Conformation of gramicidin a in water: Inference from analysis of hydrogen/deuterium exchange behavior by matrix assisted laser desorption ionization mass spectrometry. *Biopolymers* 80:708–713.

Jiang, Y., A. Lee, J. Chen, M. Cadene, B.T. Chait, and R. MacKinnon. 2002. Crystal structure and mechanism of a calcium-gated potassium channel. *Nature* 417:515–522.

Jiang, Y., A. Lee, J. Chen, V. Ruta, M. Cadene, B.T. Chait, and R. MacKinnon. 2003. X-ray structure of a voltage-dependent K^+channel. *Nature* 423:33–41.

Jing, N., K.U. Prasad, and D.W. Urry. 1995. The determination of binding constants of micellar-packaged gramicidin A by ^{13}C-and ^{23}Na-NMR. *Biochim. Biophys. Acta* 1238:1–11.

Au: Please check the name of the journal.

Au: Please check the location of the publisher.

Jing, N., and D.W. Urry. 1995. Ion pair binding of Ca^{2+} and Cl^{-} ions in micellar-packaged gramicidin A. *Biochim. Biophys. Acta* 1238:12–21.

Jordan, P.C. 1981. Energy barriers for passage of ions through channels. Exact solution of two electrostatic problems. *Biophys. Chem.* 13:203–212.

Jordan, P.C. 1984. The total electrostatic potential in a gramicidin channel. *J. Membr. Biol.* 78:91–102.

Jude, A.R., D.V. Greathouse, R.E. Koeppe II, L.L. Providence, and O.S. Andersen. 1999. Modulation of gramicidin channel structure and function by the aliphatic "spacer" residues 10, 12, and 14 between the tryptophans. *Biochemistry* 38:1030–1039.

Karplus, M., and J.A. McCammon. 1981. The internal dynamics of globular proteins. *CRC Crit. Rev. Biochem.* 9:293–349.

Katsaras, J., R.S. Prosser, R.H. Stinson, and J.H. Davis. 1992. Constant helical pitch of the gramicidin channel in phospholipid bilayers. *Biophys. J.* 61:827–830.

Kauzmann, W. 1957. Some factors in the interpretation of protein denaturation. *Adv. Protein Chem.* 14:1–63.

Kemp, G., and C. Wenner. 1976. Solution, interfacial, and membrane properties of gramicidin A. *Arch. Biochem. Biophys.* 176:547–555.

Kessler, N., H. Schuhmann, S. Morneweg, U. Linne, and M.A. Marahiel. 2004. The linear pentadecapeptide gramicidin is assembled by four multimodular nonribosomal peptide synthetases that comprise 16 modules with 56 catalytic domains. *J. Biol. Chem.* 279:7413–7419.

Ketchem, R.R., B. Roux, and T.A. Cross. 1997. High-resolution polypeptide structure in a lamellar phase lipid environment from solid state NMR derived orientational constraints. *Structure* 5:1655–1669.

Killian, J.A., S. Morein, P.C. van der Wel, M.R. de Planque, D.V. Greathouse, and R.E. Koeppe 2nd. 1999. Peptide influences on lipids. *Novartis Found. Symp.* 225:170–183; discussion 183–187.

Killian, J.A., M.J. Taylor, and R.E. Koeppe II. 1992. Orientation of the valine-1 side chain of the gramicidin transmembrane channel and implications for channel functioning. A^2 H NMR study. *Biochemistry* 31:11283–11290.

Killian, J.A., and G. von Heijne. 2000. How proteins adapt to a membrane-water interface. *TIBS* 25:429–434.

King, E.L., and C. Altman. 1956. A schematic method of deriving the rate laws for enzyme-catalyzed reactions. *J. Phys. Chem.* 60:1375–1378.

Koeppe, R.E., II, and O.S. Andersen. 1996. Engineering the gramicidin channel. *Annu. Rev. Biophys. Biomol. Struct.* 25:231–258.

Koeppe, R.E., II, D.V. Greathouse, A. Jude, G. Saberwal, L.L. Providence, and O.S. Andersen. 1994a. Helix sense of gramicidin channels as a "nonlocal" function of the primary sequence. *J. Biol. Chem.* 269:12567–12576.

Koeppe, R.E. II, J.A. Killian, and D.V. Greathouse. 1994b. Orientations of the tryptophan 9 and 11 side chains of the gramicidin channel based on deuterium nuclear magnetic resonance spectroscopy. *Biophys. J.* 66:14–24.

Koeppe, R.E., II, J.-L. Mazet, and O.S. Andersen. 1990. Distinction between dipolar and inductive effects in modulating the conductance of gramicidin channels. *Biochemistry* 29:512–520.

Koeppe, R.E., II, J.A. Paczkowski, and W.L. Whaley. 1985. Gramicidin K, a new linear channel-forming gramicidin from *Bacillus brevis*. *Biochemistry* 24:2822–2827.

Koeppe, R.E., II, H. Sun, P.C. van der Wel, E.M. Scherer, P. Pulay, and D.V. Greathouse. 2003. Combined experimental/theoretical refinement of indole ring geometry using deuterium magnetic resonance and ab initio calculations. *J. Am. Chem. Soc.* 125:12268–12276.

König, S., E. Sackmann, D. Richter, R. Zorn, C. Carlile, and T.M. Bayerl. 1994. Molecular dynamics of water in oriented DPPC multilayers studied by quasielastic neutron scattering and deuterium–nuclear magnetic resonance relaxation. *J. Chem. Phys.* 100:3307–3316.

Kramers, H.A. 1940. Brownian motion in a field of force and the diffusion model of chemical reactions. *Physica* 7:284–304.

Kuo, A., J.M. Gulbis, J.F. Antcliff, T. Rahman, E.D. Lowe, J. Zimmer, J. Cuthbertson, F.M. Ashcroft, T. Ezaki, and D.A. Doyle. 2003. Crystal structure of the potassium channel KirBac1.1 in the closed state . *Science* 300:1922–1926.

Lamoureux, G., A.D. MacKerell Jr., and B. Roux. 2003. A simple polarizable water model based on classical Drude oscillators. *J. Chem. Phys.* 5185–5197.

Lamoureux, G., and B. Roux. 2003. Modeling induced polarizability with classical Drude oscillators: Theory and molecular dynamics simulation algorithm. *J. Chem. Phys.* 3025–3039.

Langs, D.A. 1988. Three-dimensional structure at 0.86 Å of the uncomplexed form of the transmembrane ion channel peptide gramicidin A. *Science* 241:188–191.

Läuger, P. 1976. Diffusion-limited ion flow through pores. *Biochim. Biophys. Acta* 455:493–509.

Lee, K.C., S. Huo, and T.A. Cross. 1995. Lipid–peptide interface: Valine conformation and dynamics in the gramicidin channel. *Biochemistry* 34:857–867.

Levitt, D.G. 1978. Electrostatic calculations for an ion channel. I. Energy and potential profiles and interactions between ions. *Biophys. J.* 22:209–219.

Levitt, D.G., S.R. Elias, and J.M. Hautman. 1978. Number of water molecules coupled to the transport of sodium, potassium and hydrogen ions via gramicidin, nonactin or valinomycin. *Biochim. Biophys. Acta* 512:436–451.

Lewis, B.A., and D.M. Engelman. 1983. Lipid bilayer thickness varies linearly with acyl chain length in fluid phosphatidylcholine vesicles. *J. Mol. Biol.* 166:211–217.

Lindahl, E., and O. Edholm. 2000. Mesoscopic undulations and thickness fluctuations in lipid bilayers from molecular dynamics simulations. *Biophys. J.* 79:426.

Lipmann, F. 1980. Bacterial production of antibiotic polypeptides by thiol-linked synthesis on protein templates. *Adv. Microb. Physiol.* 21:227–266.

Liu, N., and R.L. Kay. 1977. Redetermination of the pressure dependence of the lipid bilayer phase transition. *Biochemistry* 16:3484–3486.

Au: Please provide the volume number, if any.

Au: Please provide the volume number, if any.

Long, S.B., E.B. Campbell, and R. Mackinnon. 2005. Crystal structure of a mammalian voltage-dependent Shaker family K^+ channel. *Science* 309:897–903.

Lundbæk, J.A., P.H.A.J. Birn, R. Søgaard, C. Nielsen, J. Girshman, M.J. Bruno, S.E. Tape, J. Egebjerg, D.V. Greathouse, G.L. Mattice, R.E. Koeppe II, and O.S. Andersen. 2004. Regulation of sodium channel function by bilayer elasticity: The importance of hydrophobic coupling: Effects of micelle-forming amphiphiles and cholesterol. *J. Gen. Physiol.* 123:599–621.

Mackay, D.H.J., P.H. Berens, K.R. Wilson, and A.T. Hagler. 1984. Structure and dynamics of ion transport through gramicidin A. *Biophys. J.* 46:229–248.

Mamanov, A.B., R.D. Coalson, A. Nitzan, and M.G. Kurnikova. 2003. The role of the dielectric barrier in narrow biological channels: A novel composite approach to modeling single-channel currents. *Biophys. J.* 84:3646–3661.

Mattice, G.L., R.E. Koeppe II, L.L. Providence, and O.S. Andersen. 1995. Stabilizing effect of D-alanine[2] in gramicidin channels. *Biochemistry* 34:6827–6837.

Mazet, J.L., O.S. Andersen, and R.E. Koeppe II. 1984. Single-channel studies on linear gramicidins with altered amino acid sequences. A comparison of phenylalanine, tryptophan, and tyrosine substitutions at positions 1 and 11. *Biophys. J.* 45:263–276.

Mobashery, N., C. Nielsen, and O.S. Andersen. 1997. The conformational preference of gramicidin channels is a function of lipid bilayer thickness. *FEBS Lett.* 412:15–20.

Morrow, J.S., W.R. Veatch, and L. Stryer. 1979. Transmembrane channel activity of gramicidin A analogs: Effects of modification and deletion of the amino-terminal residue. *J. Mol. Biol.* 132:733–738.

Mouritsen, O.G., and M. Bloom. 1984. Mattress model of lipid–protein interactions in membranes. *Biophys. J.* 46:141–153.

Mukherjee, S., and A. Chattopadhyay. 1994. Motionally restricted tryptophan environments at the peptide–lipid interface of gramicidin channels. *Biochemistry* 33:5089–5097.

Myers, V.B., and D.A. Haydon. 1972. Ion transfer across lipid membranes in the presence of gramicidin A. II. Ion selectivity. *Biochim. Biophys. Acta* 274:313–322.

Neher, E., J. Sandblom, and G. Eisenman. 1978. Ionic selectivity, saturation, and block in gramicidin A channels. II. Saturation behavior of single channel conductances and evidence for the existence of multiple binding sites in the channel. *J. Membr. Biol.* 40:97–116.

Neumcke, B., and P. Läuger. 1969. Nonlinear electrical effects in lipid bilayer membranes II. Integration of the generalized Nernst–Planck equations. *Biophys. J.* 9:1160–1170.

Nicholson, L.K., F. Moll, T.E. Mixon, P.V. LoGrasso, J.C. Lay, and T.A. Cross. 1987. Solid-state 15N NMR of oriented lipid bilayer bound gramicidin A'. *Biochemistry* 26:6621–6626.

Nielsen, C., M. Goulian, and O.S. Andersen. 1998. Energetics of inclusion-induced bilayer deformations. *Biophys. J.* 74:1966–1983.

Nielsen, C., and O.S. Andersen. 2000. Inclusion-induced bilayer deformations: Effects of monolayer equilibrium curvature. *Biophys. J.* 79:2583–2604.

Nimigean, C.M., and C. Miller. 2002. Na^+ block and permeation in a K^+ channel of known structure. *J. Gen. Physiol.* 120:323.

Noskov, S.Y., S. Bernèche, and B. Roux. 2004. Control of ion selectivity in potassium channels by electrostatic and dynamic properties of carbonyl ligands. *Nature* 431:830–834.

O'Connell, A.M., R.E. Koeppe II, and O.S. Andersen. 1990. Kinetics of gramicidin channel formation in lipid bilayers: Transmembrane monomer association. *Science* 250:1256–1259.

Oiki, S., R.E. Koeppe II, and O.S. Andersen. 1994. Asymmetric gramicidin channels. Heterodimeric channels with a single F^6 Val^1 residue. *Biophys. J.* 66:1823–1832.

Oiki, S., R.E. Koeppe II, and O.S. Andersen. 1995. Voltage-dependent gating of an asymmetric gramicidin channel. *Proc. Natl. Acad. Sci. USA* 92:2121–2125.

Olah, G.A., H.W. Huang, W.H. Liu, and Y.L. Wu. 1991. Location of ion-binding sites in the gramicidin channel by X-ray diffraction. *J. Mol. Biol.* 218:847–858.

Owicki, J.C., M.W. Springgate, and H.M. McConnell. 1978. Theoretical study of protein–lipid and protein–protein interactions in bilayer membranes. *Proc. Natl. Acad. Sci. USA* 75:1616–1619.

Park, J.B., H.J. Kim, P.D. Ryu, and E. Moczydlowski. 2003. Effect of phosphatidylserine on unitary conductance and Ba^{2+} block of the BK Ca^{2+}-activated K^+ channel: Re-examination of the surface charge hypothesis. *J. Gen. Physiol.* 121:375–398.

Parsegian, A. 1969. Energy of an ion crossing a low dielectric membrane: Solutions to four relevant electrostatic problems. *Nature* 221:844–846.

Providence, L.L., O.S. Andersen, D.V. Greathouse, R.E. Koeppe II, and R. Bittman. 1995. Gramicidin channel function does not depend on phospholipid chirality. *Biochemistry* 34:16404–16411.

Pulay, P., E.M. Scherer, P.C. van der Wel, and R.E. Koeppe II. 2005. Importance of tensor asymmetry for the analysis of 2H NMR spectra from deuterated aromatic rings. *J. Am. Chem. Soc.* 127:17488–17493.

Ramachandran, G.N., and R. Chandrasekaran. 1972. Studies on dipeptide conformation and on peptides with sequences of alternating L and D residues with special reference to antibiotic and ion transport peptides. *Progr. Pept. Res.* 2:195–215.

Rawat, S.S., D.A. Kelkar, and A. Chattopadhyay. 2004. Monitoring gramicidin conformations in membranes: A fluorescence approach. *Biophys. J.* 87:831–843.

Rawicz, W., K.C. Olbrich, T. McIntosh, D. Needham, and E. Evans. 2000. Effect of chain length and unsaturation on elasticity of lipid bilayers. *Biophys. J.* 79:328–339.

Robinson, R.A., and R.H. Stokes. 1959. Electrolyte Solutions, 2nd Ed. Butterworth, London.

Rosenberg, P.A., and A. Finkelstein. 1978. Interaction of ions and water in gramicidin A channels: Streaming potentials across lipid bilayer membranes. *J. Gen. Physiol.* 72:327–340.

Roux, B. 2002. Computational studies of the gramicidin channel. *Acc. Chem. Res.* 35:366–375.

Roux, B., T.W. Allen, S. Bernèche, and W. Im. 2004. Theoretical and computational models of biological ion channels. *Q. Rev. Biophys.* 37:15–103.

Roux, B., and M. Karplus. 1993. Ion transport in the gramicidin channel: Free energy of the solvated right-handed dimer in a model membrane. *J. Am. Chem. Soc.* 115:3250–3262.

Roux, B., B. Prod'hom, and M. Karplus. 1995. Ion transport in the gramicidin channel: Molecular dynamics study of single and double occupancy. *Biophys. J.* 68:876–892.

Russell, E.W.B., L.B. Weiss, F.I. Navetta, R.E. Koeppe II, and O.S. Andersen. 1986. Single-channel studies on linear gramicidins with altered amino acid side chains. Effects of altering the polarity of the side chain at position 1 in gramicidin A. *Biophys. J.* 49:673–686.

Salom, D., M.C. Bańo, L. Braco, and C. Abad. 1995. HPLC demonstration that an all Trp→Phe replacement in gramicidin A results in a conformational rearrangement from beta-helical monomer to double-stranded dimer in model membranes. *Biochem. Biophys. Res. Commun.* 209:466–473.

Salom, D., E. Perez-Paya, J. Pascal, and C. Abad. 1998. Environment- and sequence-dependent modulation of the double-stranded to single-stranded conformational transition of gramicidin A in membranes. *Biochemistry* 37:14279–14291.

Sancho, M., and G. Martinez. 1991. Electrostatic modeling of dipole–ion interactions in gramicidin like channels. *Biophys. J.* 60:81–88.

Sarges, R., and B. Witkop. 1965. Gramicidin A. V. The structure of valine- and isoleucine-gramicidin A. *J. Am. Chem. Soc.* 87:2011–2019.

Scarlata, S.F. 1988. The effects of viscosity on gramicidin tryptophan rotational motion. *Biophys. J.* 54:1149–1157.

Schagina, L.V., A.E. Grinfeldt, and A.A. Lev. 1978. Interaction of cation fluxes in gramicidin A channels in lipid bilayer membranes. *Nature* 273:243–245.

Schatzberg, P. 1965. Diffusion of water through hydrocarbon liquids. *J. Polym. Sci. C* 10:87–92.

Schiffer, M., C.-H. Chang, and F.J. Stevens. 1992. The functions of tryptophan residues in membrane proteins. *Protein Engng.* 5:213–214.

Schracke, N., U. Linne, C. Mahlert, and M.A. Marahiel. 2005. Synthesis of linear gramicidin requires the cooperation of two independent reductases. *Biochemistry* 44:8507–8513.

Segrest, J.P., and R.J. Feldmann. 1974. Membrane proteins: Amino acid sequence and membrane penetration. *J. Mol. Biol.* 87:853–858.

Separovic, F., R. Pax, and B. Cornell. 1993. NMR order parameter analysis of a peptide plane aligned in a lyotropic liquid crysta. *Mol. Phys.* 78:357–369.

Sham, S.S., S. Shobana, L.E. Townsley, J.B. Jordan, J.Q. Fernandez, O.S. Andersen, D.V. Greathouse, and J.F. Hinton. 2003. The structure, cation binding, transport, and conductance of Gly15-gramicidin A incorporated into SDS micelles and PC/PG vesicles. *Biochemistry* 42:1401–1409.

Sharp, K.A., A. Nicholls, R.F. Fine, and B. Honig. 1991. Reconciling the magnitude of the microscopic and macroscopic hydrophobic effects. *Science* 252:106–109.

Sieber, S.A., and M.A. Marahiel. 2005. Molecular mechanisms underlying nonribosomal peptide synthesis: Approaches to new antibiotics. *Chem. Rev.* 105:715–738.

Simon, S.A., and T.J. McIntosh. 1986. Depth of water penetration into lipid bilayers. *Methods Enzymol.* 127:511–521.

Smyth, C.P. 1955. Dielectric Behavior and Structure. Mcgraw-Hill, New York.

Tanford, C. 1980. The Hydrophobic Effect: Formation of Micelles and Biological Membranes, 2nd Ed. Wiley, New York.

Tian, F., and T.A. Cross. 1999. Cation transport: An example of structural based selectivity. *J. Mol. Biol.* 285:1993–2003.

Tosh, R.E., and P.J. Collings. 1986. High pressure volumetric measurements in dipalmitoylphosphatidylcholine bilayers. *Biochim. Biophys. Acta* 859:10–14.

Townsley, L.E., W.A. Tucker, S. Sham, and J.F. Hinton. 2001. Structures of gramicidins A, B, and C incorporated into sodium dodecyl sulfate micelles. *Biochemistry* 40:11676–11686.

Unwin, N. 2005. Refined structure of the nicotinic acetylcholine receptor at 4 Å resolution. *J. Mol. Biol.* 346:967–989.

Urban, B.W., S.B. Hladky, and D.A. Haydon. 1978. The kinetics of ion movements in the gramicidin channel. *Fed. Proc.* 37:2628–2632.

Urban, B.W., S.B. Hladky, and D.A. Haydon. 1980. Ion movements in gramicidin pores. An example of single-file transport. *Biochim. Biophys. Acta* 602:331–354.

Urry, D.W. 1971. The gramicidin A transmembrane channel: A proposed $\pi_{(L,D)}$ helix. *Proc. Natl. Acad. Sci. USA* 68:672–676.

Urry, D.W. 1972. Protein conformation in biomembranes: Optical rotation and absorption of membrane suspensions. *Biochim. Biophys. Acta* 265:115–168.

Urry, D.W. 1973. Polypeptide conformation and biological function: β-helices ($\pi_{L,D}$-helices) as permselective transmembrane channels. *Jerusalem Symp. Quant. Chem. Biochem.* 5:723–736.

Urry, D.W., S. Alonso-Romanowski, C.M. Venkatachalam, R.J. Bradley, and R.D. Harris. 1984. Temperature dependence of single channel currents and the peptide libration mechanism for ion transport through the gramicidin A transmembrane channel. *J. Membr. Biol.* 81:205–217.

Urry, D.W., T.L. Trapane, C.M. Venkatachalam, and R.B. McMichens. 1989. Ion interactions at membranous polypeptide sites using nuclear magnetic resonance: Determining rate and binding constants and site locations. *Methods Enzymol.* 171:286–342.

Urry, D.W., T.L. Trapane, J.T. Walker, and K.U. Prasad. 1982. On the relative lipid membrane permeability of Na^+ and Ca^{2+}. A physical basis for the messenger role of Ca^{2+}. *J. Biol. Chem.* 257:6659–6661.

Veatch, W., and L. Stryer. 1977. The dimeric nature of the gramicidin A transmembrane channel: Conductance and fluorescence energy transfer studies of hybrid channels. *J. Mol. Biol.* 113:89–102.

Veatch, W.R., and E.R. Blout. 1974. The aggregation of gramicidin A in solution. *Biochemistry* 13:5257–5264.

Veatch, W.R., E.T. Fossel, and E.R. Blout. 1974. The conformation of gramicidin A. *Biochemistry* 13:5249–5256.

Wallace, B.A., W.R. Veatch, and E.R. Blout. 1981. Conformation of gramicidin A in phospholipid vesicles: Circular dichroism studies of effects of ion binding, chemical modification, and lipid structure. *Biochemistry* 20:5754–5760.

Weinstein, S., B.A. Wallace, E.R. Blout, J.S. Morrow, and W. Veatch. 1979. Conformation of gramicidin A channel in phospholipid vesicles: A carbon-13 and fluorine-19 nuclear magnetic resonance study. *Proc. Natl. Acad. Sci. USA* 76:4230–4234.

Weinstein, S., B.A. Wallace, J.S. Morrow, and W.R. Veatch. 1980. Conformation of the gramicidin A transmembrane channel: A 13C nuclear magnetic resonance study of 13C-enriched gramicidin in phosphatidylcholine vesicles. *J. Mol. Biol.* 143:1–19.

Weiss, L.B., and R.E. Koeppe II. 1985. Semisynthesis of linear gramicidins using diphenyl phosphorazidate (DPPA). *Int. J. Pept. Protein Res.* 26:305–310.

Weiss, M.S., A. Kreusch, E. Schiltz, U. Nestel, W. Welte, J. Weckesser, and G.E. Schulz. 1991. The structure of porin from *Rhodobacter capsulatus* at 1.8 Å resolution. *FEBS Lett.* 280:379–382.

White, S.H., and W.C. Wimley. 1999. Membrane protein folding and stability: Physical principles. *Annu. Rev. Biophys. Biomol. Struct.* 28:319–365.

Wiener, M.C., and S.H. White. 1992. Structure of a fluid dioleoylphosphatidylcholine bilayer determined by joint refinement of x-ray and neutron diffraction data. III. Complete structure. *Biophys. J.* 61:437–447.

Wolfenden, R., and M.J. Snider. 2001. The depth of chemical time and the power of enzymes as catalysts. *Acc. Chem. Res.* 12:938–945.